Acta Mechanica (2006)
DOI 10.1007/s00707-005-0293-4

Acta Mechanica
Printed in Austria

Stokes flow through a channel with wavy walls

A. E. Malevich, Minsk, Belarus, **V. V. Mityushev**, Krakow, Poland, and
P. M. Adler, Paris, France

Received September 13, 2005
Published online: March 6, 2006

Summary. Stokes flow is solved through a channel with three-dimensional wavy walls enclosed by two wavy walls whose amplitude is proportional to the mean clearance of the channel multiplied by the small dimensionless parameter ε. The application of an analytical-numerical algorithm yields efficient formulas for the velocities and permeability. These formulas include ε in symbolic form. When ε increases, the Poiseuille flow ($\varepsilon = 0$) is disturbed and eddies can arise above a critical value $\varepsilon = \varepsilon_e$. These results are also successfully compared to the ones derived by a fully numerical solution.

1 Introduction

The present paper is devoted to the flow of a viscous fluid through a channel (see Figs. 1 and 2) under the assumption that the Reynolds number is small enough for a Stokes flow approximation to be made. The classical Poiseuille flow in the channel bounded by two parallel planes arises when a pressure gradient $\overline{\nabla p}$ is applied. The flow profile obeys the well-known parabolic law. The influence of curvilinear edges on flow is of fundamental interest since it illustrates the mechanism of viscous flow under different geometrical conditions. Apart from its theoretical importance, the flow through curvilinear channels has application in porous media [1]–[5].

Many studies addressed two-dimensional channels with sinusoidal walls. Burns and Parkes [6] considered two-dimensional flow through a symmetrical channel bounded by the surfaces

$$z = \pm b(1 + \varepsilon \cos x). \tag{1}$$

The notations are explained in Fig. 2. The problem was solved by expanding the stream function in a Fourier series involving an infinite set of unknown coefficients. Burns and Parkes obtained a perturbation solution in which these Fourier coefficients were calculated up to $O(\varepsilon^6)$. Wang [7] obtained a similar result for channels bounded by $z = \pm 1 \pm \varepsilon \sin \alpha x \sin \beta y$, but he limited his expansion to $O(\varepsilon)$ for the velocity and to $O(\varepsilon^2)$ for the averaged velocity which is somewhat trivial.

The case of a curvilinear tube with a radius which varies sinusoidally in the axial direction, was studied by Deiber and Schowalter [8] by the method of separated variables. The corresponding ordinary differential equations were solved by a finite difference method. Hasegawa and Izuchi [9], [10] studied the Navier-Stokes equations and they assumed that the walls of the channel were sufficiently close. They constructed an iterative scheme based on linear differential equations. An analytical formula for the flow rate was obtained for sinusoidal channels up to $O(\varepsilon^6)$. Recently, Floryan [11] solved the Navier-Stokes equations in a

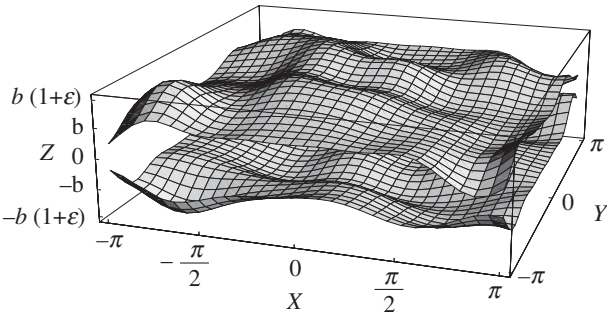

Fig. 1. Example of a channel bounded by three-dimensional solid surfaces

two-dimensional symmetric sinusoidal channel; expanding the stream function into Fourier series, he reduced the problem to an infinite nonlinear system of differential equations and solved this system numerically. The linear stability of flow was analyzed for large Reynolds numbers.

Mourzenko et al. [3], [4] studied the permeability of self-affine fractures by direct three-dimensional simulations. They also addressed the case where the aperture of the channel vanishes on a significant part of the whole channel. A relation between the permeability, the fractional open area and the percolation probability was derived.

The structure of the flow in curvilinear channels essentially depends on the wave amplitude of the walls. The flow in some channels is separated into a series of flow cells. In the middle part of the channel, the velocity profiles look like a disturbed Poiseuille parabolic profile. The flow near the walls can be similar to the flow in a cavity where developed viscous eddies arise. These eddies are characterized by a change of the vorticity sign. Systematical studies of eddies were performed by Moffatt in his seminal paper [12] where he proved that any flow at the corner between two planes consists of a sequence of self-similar eddies, when the angle between the planes is less than a critical value. One can find recent results devoted to this topic in [13] and [14]. The boundary-integral method was applied by Pozrikidis [15] to two-dimensional channels; a general numerical procedure was described and applied to a channel constricted by plane and sinusoidal walls where the onset of reversed-flow regions was observed when the wave amplitude of the boundary exceeds a critical value; onset of eddies was explained in terms of [12].

Scholle et al. [16], [17] studied gravity-driven flows on an inclined sinusoidal bottom. This study is based on the series representation of the stream function

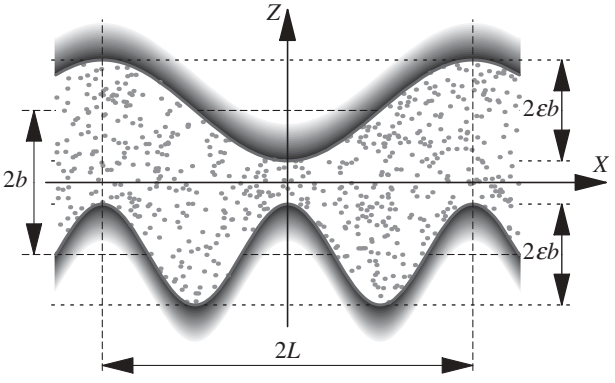

Fig. 2. Schematic diagram for the major notations. The three axes are denoted by x, y and z; the average pressure gradient is usually parallel to the x–axis; the transversal coordinate is z. The average aperture is equal to $2b$.

$$\psi(x,z) = Az^2 + Bz^3 + \sum_{n=-\infty}^{+\infty} e^{-nz}[(R_n + zQ_n)e^{-inx} + c.c.]. \tag{2}$$

Using the no-slip condition, Scholle et al. [16], [17] deduced an infinite set of linear algebraic equations for the coefficients R_n and Q_n. The set is solved by the truncation method. The results were used to investigate the generation and evolution of eddies as a function of waviness, dimensionless film thickness, inclination angle and capillary number. The number and size of eddies were shown to increase with wall waviness and film thickness. The theoretical results of Scholle et al. [16], [17] are in excellent agreement with the experiments performed by Wierschem et al. [18] and Gaskell [19], who demonstrated that the validity of the lubrication approximation is restricted to weakly undulated walls.

Recently, Zhou et al. [20] considered a flow governed by the stationary Navier-Stokes equations inside two-dimensional channels using perturbations on ε up to $O(\varepsilon^2)$. The flow was examined for sinusoidal, arched and triangular profiles of the walls. The authors have also derived the critical Reynolds number at which eddies first occur. Bontozoglou [21] numerically studied by a spectral discretization method the gravity–driven flow as a function of the film Reynolds number and of the wall amplitude.

Other theoretical and experimental investigations close to the present topic are reported in the references of the literature cited above (for instance, flow in a pipe of circular cross-section [6], Couette flow [15], gravity-driven flow [16], [17], [19], [21] and theoretical and experimental investigations of the critical Reynolds number [18], [20].

Our main objective in the present work is to study the dependence of flow in channels on ε: (i) to study the permeability as a function of ε; (ii) to determine the critical value ε_e when eddies arise. Application of the method of perturbation on ε is an efficient way to establish these dependences. Numerical computations performed in the previous works give us only limited views of the complex dependence of the flow on ε.

In this paper, we develop a general asymptotic analysis and apply it to curvilinear three-dimensional channels bounded by walls of the form (cf. Figs. 1 and 2)

$$z = S^+(x,y) \equiv b(1 + \varepsilon T(x,y)), \tag{3}$$

$$z = S^-(x,y) \equiv -b(1 + \varepsilon B(x,y)). \tag{4}$$

We consider arbitrary profiles $S^{\pm}(x,y)$ satisfying some natural conditions. For definiteness, we assume that

$$|T(x,y)| \leqslant 1 \quad \text{and} \quad |B(x,y)| \leqslant 1. \tag{5}$$

For infinitely differentiable functions $T(x,y)$ and $B(x,y)$, we have deduced in Subsect. 3.1 a cascade of boundary value problems for the Stokes equations for a straight channel to calculate velocities and permeability in the form of an ε-expansion. In Subsect. 3.2, we have constructed an analytical solver which is applied to each step of the cascade. The convergence of the proposed algorithm is justified in Appendix A. We have established that the ε-expansion of the velocities converges if ε does not exceed the critical value $\varepsilon_c = (b\varkappa)^{-1}$ where $\varkappa$ is the maximal wave number of the trigonometric polynomials $T(x,y)$ and $B(x,y)$. The refinement formula (A.1) for ε_c is deduced for general functions $T(x,y)$ and $B(x,y)$.

In Subsect. 3.3, we have deduced the efficient formula (55) for the channel permeability K. More precisely, this formula determines the coefficients of a Taylor expansion $K(\varepsilon) = \sum_{m=0}^{\infty} K_m \varepsilon^m$ (normalization (17) is used for K). In practical computations $K(\varepsilon)$ is approximated by the Taylor polynomial $K_N(\varepsilon) = \sum_{m=0}^{N} K_m \varepsilon^m$. However, the domain of application of this formula is restricted, since the corresponding Taylor series can be divergent for

$\varepsilon \geq \varepsilon_c$. Then, using Padé approximations [24] which transform a polynomial to a rational function, we obtain $K(\varepsilon) \approx P_m(\varepsilon)/Q_n(\varepsilon)$, where $P_m(\varepsilon)$ and $Q_n(\varepsilon)$ are polynomials ($m+n=N$). In this representation complex poles of $K(\varepsilon)$, blocking the convergence, are placed into zeros of $Q_n(\varepsilon)$. Padé approximations are also applied to calculation of velocity. It is worth noting that eddies can arise only if $\varepsilon > \varepsilon_c$ for Poiseuille flow. Hence, it was impossible to note eddies in the previous works based on the ε-expansion.

A few examples of two- and three-dimensional channels are gathered in Sect. 4 and they illustrate various aspects of our methodology and its specific advantages. The two first cases are two-dimensional with either symmetric or antisymmetric walls. The third example is three-dimensional and it illustrates the power of our methodology since an expansion up to $O(\varepsilon^{14})$ is readily derived. The last two subsections address the onset of eddies in two-dimensional channels.

In Sect. 5, we have obtained an analytical formula for the permeability up to $O(\varepsilon^4)$ for two-dimensional channels with arbitrary boundaries including fractal surfaces; the precise mathematical justification is given in Appendix B. In Sect. 6, the classical lubrication approximation is revisited.

In Sect. 7, some concluding remarks are given. They summarize the advantages of the present methodology and the various applications that we envision.

2 Statement of the problem

Let the profiles $S^{\pm}$ be determined respectively by Eqs. (3) and (4) where the functions $T(x,y)$ and $B(x,y)$ are defined in the square $[-L,L]\times[-L,L]$ of the plane XOY. We assume that T and B can be periodically continued onto the whole plane XOY, and that the functions T and B are infinitely differentiable everywhere on XOY. In Sect. 5, the latter condition will be weakened. In Eqs. (3) and (4), ε is formally defined as a small parameter because we use expansions in ε around the point $\varepsilon = 0$. For definiteness, we take $\varepsilon > 0$.

Without any loss of generality, we assume that

$$\int_{-L}^{L}\int_{-L}^{L} T(x,y)dx\,dy = \int_{-L}^{L}\int_{-L}^{L} B(x,y)dx\,dy = 0, \tag{6}$$

i.e., the mean amplitudes of T with respect to the plane $z=b$, and of B with respect to $z=-b$, are equal to zero. The channel has a spatially periodic structure and is made of unit cells defined as

$$Q := \left\{(x,y,z)\in\mathbb{R}^3 :\ -L\leq x\leq L,\ -L\leq y\leq L,\ S^-(x,y) < z < S^+(x,y)\right\}.$$

Let $\mathbf{u}=\mathbf{u}(x,y,z)$ be the velocity vector, and $p=p(x,y,z)$ the pressure. The fluid is governed by the Stokes equations

$$\begin{aligned} &\mu\nabla^2\mathbf{u} = \nabla p,\\ &\nabla\cdot\mathbf{u} = \mathbf{0} \end{aligned} \tag{7}$$

with the boundary conditions

$$\mathbf{u} = \mathbf{0} \qquad \text{on } S^{\pm}. \tag{8}$$

The solution $\mathbf{u}$ of Eqs. (7)–(8) belongs to the class of periodic functions with period $2L$ in x and y. We apply an overall external gradient pressure $\overline{\nabla p}$ along the x-direction. It can be described by a constant jump $2L\overline{\nabla p}$ along the x-axis of the periodic cell

$$p(x+L,y,z)-p(x-L,y,z)=2L\overline{\nabla p}. \tag{9}$$

Let $\mathbf{u}$ be a solution of the problem (7)–(9), and let u be the x-component of $\mathbf{u}$. The permeability of the channel in the x-direction is defined as

$$K_x(\varepsilon)=-\frac{\mu}{\overline{\nabla p}\,|\tau|}\int_{-L}^{L}\int_{-L}^{L}dx\,dy\int_{S^-(x,y)}^{S^+(x,y)}u(x,y,z)dz, \tag{10}$$

where $|\tau|$ is the volume of the unit cell Q of the channel,

$$|\tau|=\int_{-L}^{L}\int_{-L}^{L}dx\,dy\int_{S^-(x,y)}^{S^+(x,y)}dz=8bL^2. \tag{11}$$

The integral (11) is calculated with the help of Eq. (6). $K_x(\varepsilon)$ in Eq. (10) is considered as a function in ε. The case $\varepsilon=0$ corresponds to the Poiseuille flow for which Eq. (10) yields the permeability

$$K_x(0)=\frac{b^2}{3}. \tag{12}$$

For convenience, we introduce dimensionless quantities that are indicated by primes:

$$(x,y,z)=\frac{L}{\pi}(x',y',z'),\quad \mathbf{u}=\frac{L^2\overline{\nabla p}}{2\mu\pi^2}\mathbf{u}',\quad p=\frac{L\overline{\nabla p}}{2\pi}p',\quad K_x(\varepsilon)=\frac{L^2}{2\pi^2}\,K_x'(\varepsilon). \tag{13}$$

Equations (7)–(9) take the following dimensionless form:

$$\begin{aligned}&\nabla'^2\mathbf{u}'=\nabla' p',\\&\nabla'\cdot\mathbf{u}'=\mathbf{0},\end{aligned} \tag{14}$$

and

$$p'(x'+\pi,y',z')-p'(x'-\pi,y',z')=-4\pi. \tag{15}$$

Then, the velocity $\mathbf{u}'$ for Poiseuille flow ($\varepsilon=0$) becomes

$$\mathbf{u}_0'(x',y',z')=\big(b'^2-z'^2,0,0\big), \tag{16}$$

where $b'=\frac{\pi b}{L}$. Further, we define the ratio $K=K(\varepsilon)$ between the dimensional permeabilities of the curvilinear channel and of the Poiseuille flow,

$$K(\varepsilon)=\frac{K_x'(\varepsilon)}{K_x'(0)}=\frac{K_x(\varepsilon)}{K_x(0)}. \tag{17}$$

In the present paper, we use the dimensionless variables $\mathbf{u}'$, p' and the normalized permeability $K(\varepsilon)$. Below the primes in the dimensionless coordinates, b', velocity and pressure are omitted. We also use the notations (3) and (4) for the dimensionless geometric parameters.

3 General solution

3.1 General algorithm

The following treatment is very close to the determination of the resistance of a slightly deformed sphere by Happel and Brenner [22] by a method of perturbation on ε. It was applied for instance to steady diffusion in a plane channel [1] (see also [23]). Let us express the velocity and the pressure as the expansions

$$\begin{aligned} p(x,y,z) &= \sum_{m=0}^{\infty} p_m(x,y,z)\varepsilon^m, \\ \mathbf{u}(x,y,z) &= \sum_{m=0}^{\infty} \mathbf{u}_m(x,y,z)\varepsilon^m. \end{aligned} \tag{18}$$

The representations (18) are justified in Appendix A where it is proved that Eq. (18) holds when ε does not exceed a critical value $(b\varkappa)^{-1}$; $\varkappa$ denotes the maximal oscillation frequency of $T(x,y)$ and $B(x,y)$.

We use the Taylor expansion for any function $g(x,y,z)$ infinitely differentiable with respect to z on the boundary surfaces $S^{\pm}$ of the channel

$$g(x,y,\pm b(1+\varepsilon S(x,y))) = \sum_{m=0}^{\infty} \frac{(\pm b)^m}{m!} S^m(x,y)\varepsilon^m \frac{\partial^m g}{\partial z^m}\Big|_{z=\pm b}. \tag{19}$$

Use of Eq. (19) for each $\mathbf{u}_m$ in Eq. (18) yields

$$\mathbf{u}(x,y,b(1+\varepsilon T(x,y))) = \sum_{m=0}^{\infty} \varepsilon^m \sum_{n=0}^{m} \frac{b^n}{n!} T^m(x,y) \frac{\partial^n \mathbf{u}_{m-n}}{\partial z^n}\Big|_{z=b}. \tag{20}$$

An analogous formula holds for $\mathbf{u}$ on S^{-}

$$\mathbf{u}(x,y,-b(1+\varepsilon B(x,y))) = \sum_{m=0}^{\infty} \varepsilon^m \sum_{n=0}^{m} \frac{(-b)^n}{n!} B^n(x,y) \frac{\partial^n \mathbf{u}_{m-n}}{\partial z^n}\Big|_{z=-b}. \tag{21}$$

Substituting Eqs. (18), (20) and (21) into (14)–(15), we obtain the following cascade of boundary value problems for the Stokes equations in the straight channel $-b < z < b$:

$$\begin{aligned} \nabla^2 \mathbf{u}_m &= \nabla p_m, \\ \nabla \cdot \mathbf{u}_m &= \mathbf{0} \end{aligned} \tag{22}$$

with the boundary conditions

$$\begin{aligned} \mathbf{u}_m(x,y,b) &= -\sum_{n=1}^{m} \frac{(bT)^n}{n!} \frac{\partial^n \mathbf{u}_{m-n}}{\partial z^n}\Big|_{z=b}, \\ \mathbf{u}_m(x,y,-b) &= -\sum_{n=1}^{m} \frac{(-bB)^n}{n!} \frac{\partial^n \mathbf{u}_{m-n}}{\partial z^n}\Big|_{z=-b}. \end{aligned} \tag{23}$$

The zeroth approximation of the velocity has the form (16). One can see that in each step m we have to solve the Stokes equations (22) with the boundary conditions (23) in which $\mathbf{u}_0$ has the form (16) and that $\mathbf{u}_1, \mathbf{u}_2, \ldots, \mathbf{u}_{m-1}$ are constructed in the previous steps. It should be noticed that in each step we solve a problem with infinitely differentiable data. Therefore, we obtain a solution preserving this property in $-b \leqslant z \leqslant b$.

3.2 Solver for the straight channel

In the previous subsection, we reduced the problem (14)–(15) for the curvilinear channel to a cascade of problems for the straight channel $-b < z < b$. Thus, we need an efficient solver for the latter problem which we rewrite as the Stokes equations

$$\begin{aligned} &\nabla^2 \mathbf{v} = \nabla q, \\ &\nabla \cdot \mathbf{v} = \mathbf{0}, \quad -b<z<b, \end{aligned} \tag{24}$$

with the boundary conditions

$$\begin{aligned} &\mathbf{v}(x,y,b) = \mathbf{f}(x,y), \\ &\mathbf{v}(x,y,-b) = \mathbf{g}(x,y). \end{aligned} \tag{25}$$

In the following two subsections we give an introductory example in details and construct a solver of the general problem (24)–(25) which is based on the method of separated variables and on double Fourier series.

a. An introductory example

In order to present the main ideas and the reduction of the problem (24)–(25) for partial differential equations to a problem of ordinary differential equations, we consider in this subsection a simple two-dimensional situation. First, we assume the following forms for the given boundary functions $\mathbf{f} = (f_1, f_2)$ and $\mathbf{g} = (g_1, g_2)$:

$$\begin{aligned} &f_1(x) = \sum_{s=1}^{\infty} f_s^{(1)} (\sin sx)_x, \quad f_2(x) = \sum_{s=1}^{\infty} f_s^{(2)} \sin sx, \\ &g_1(x) = \sum_{s=1}^{\infty} g_s^{(1)} (\sin sx)_x, \quad g_2(x) = \sum_{s=1}^{\infty} g_s^{(2)} \sin sx, \end{aligned} \tag{26}$$

where $(\sin sx)_x = \frac{\partial}{\partial x}(\sin sx)$. In such a case, the solutions $\mathbf{v} = (v_1, v_2)$ and q of the problem (24)–(25) can be found in the form

$$v_1(x,z) = \sum_{s=1}^{\infty} \alpha_s(z)(\sin sx)_x, \quad v_2(x,z) = \sum_{s=1}^{\infty} \gamma_s(z) \sin sx, \quad q(x,z) = \sum_{s=1}^{\infty} \delta_s(z) \sin sx. \tag{27}$$

Substitution of Eqs. (26) and (27) into the first component of Eq. (24) yields

$$\sum_{s=1}^{\infty} (-s^2 \alpha_s(z) + \alpha_s''(z))(\sin sx)_x = \sum_{s=1}^{\infty} \delta_s(z)(\sin sx)_x. \tag{28}$$

Therefore,

$$\alpha_s'' - s^2 \alpha_s - \delta_s = 0, \quad s = 1, 2, \ldots. \tag{29}$$

The two other components of Eq. (24) yield in a similar way

$$\gamma_s'' - s^2 \gamma_s - \delta_s' = 0, \tag{30}$$

$$\gamma_s' - s^2 \alpha_s = 0. \tag{31}$$

Equations (29)–(31) form the required system of ordinary differential equations with constant coefficients.

Substitute now Eqs. (26) and (27) into the boundary conditions (25). The first component of Eq. (25) becomes

$$\sum_{s=1}^{\infty} \alpha_s(b)(\sin sx)_x = \sum_{s=1}^{\infty} f_s^{(1)}(\sin sx)_x, \tag{32}$$

or equivalently,

$$\alpha_s(b) = f_s^{(1)}, \quad s = 1, 2, \ldots. \tag{33}$$

Along similar lines, we obtain

$$\gamma_s(b) = f_s^{(2)}, \quad \alpha_s(-b) = g_s^{(1)}, \quad \gamma_s(-b) = g_s^{(2)}. \tag{34}$$

To summarize, the ordinary differential equations (29)–(31) must satisfy the boundary conditions (33)–(34).

In order to solve the latter problem, we differentiate Eq. (29) and subtract Eq. (30) from the result:

$$\alpha_s''' - \gamma_s'' - s^2\alpha_s' + s^2\gamma_s = 0. \tag{35}$$

Next, we find from Eq. (31)

$$\alpha_s = s^{-2}\gamma_s' \tag{36}$$

and substitute it into Eq. (35):

$$s^{-2}\gamma_s^{(IV)} - 2\gamma_s'' + s^2\gamma_s = 0. \tag{37}$$

The general solution of Eq. (37) has the well-known form

$$\gamma_s(z) = (C_1 z + C_2)\cosh sz + (C_3 z + C_4)\sinh sz. \tag{38}$$

The constants $C_1, \ldots, C_4$ can be found from the boundary conditions (33)–(34) and the relation (36). The final formulas are given in the next subsection for the general three-dimensional case.

Along similar lines, one can solve the problem (24)–(25), when the first components of the boundary functions **f** and **g** are sines and the second components are cosines. The general two-dimensional case is considered by a linear combination of these two elementary cases.

b. General case

The same techniques can be used to solve the general three-dimensional problem (24)–(25), but we have to perform significantly more calculations, since we have to deal with double Fourier series when the number of the basic terms is four. In order to unify computations for all terms, it is convenient to introduce the functions

$$\mathrm{trig}_{st}(R, S, T_1, T_2; x, y) := R\cos(sx + ty) + S\sin(sx + ty) + T_1\cos(sx - ty) + T_2\sin(sx - ty). \tag{39}$$

The function trig replaces all combinations of sin and cos in the double Fourier series; of course, trig is an abbreviation of trigonometric. It is more convenient in the following algorithm because it is invariant under some differential operators; it unifies all calculations and shortens the expressions.

Let us write the known vector-function **f** from the boundary condition (25) in the form

$$\begin{aligned}\mathbf{f}(x, y) = \sum_{s,t=0}^{\infty} \Bigg(& a_{st}^{+} \frac{\partial \mathrm{trig}_{st}(R_{st}, S_{st}, T_{1st}, T_{2st}; x, y)}{\partial x}, \\ & b_{st}^{+} \frac{\partial \mathrm{trig}_{st}(R_{st}, S_{st}, T_{1st}, T_{2st}; x, y)}{\partial y}, c_{st}^{+}\mathrm{trig}_{st}(R_{st}, S_{st}, T_{1st}, T_{2st}; x, y)\Bigg),\end{aligned} \tag{40}$$

where a_{st}^{+}, b_{st}^{+}, c_{st}^{+} are constants. Note the notational shortcut; the summation applies to each of the components of the parenthesis. This is a usual double Fourier series. This particular form was chosen since it will simplify as much as possible the representation (46).

Let us explain how one obtains the representation (40) from a Fourier series in standard form. For instance, let us take the term

$$c_{st}\cos(sx+ty)=\mathrm{trig}_{st}(c_{st},0,0,0;x,y). \tag{41}$$

Applying the operators $\frac{\partial}{\partial x}$ and $\frac{\partial}{\partial y}$ to Eq. (41), we generate a triplet

$$(-c_{st}s\sin(sx+ty),-c_{st}t\sin(sx+ty),c_{st}\cos(sx+ty)). \tag{42}$$

If we put $a_{st}^{+}=-s$, $b_{st}^{+}=-t$, $c_{st}^{+}=1$, we obtain a term from Eq. (40). The representation (40) is not unique for a given $\mathbf{f}$, since instead of the Fourier coefficients f_{st} of the first coordinate of $\mathbf{f}$ we use the product $f_{st}=a_{st}^{+}R_{st}$. The same rule is used for the other coordinates. The latter is convenient for symbolic computations, because we do not care about normalization of the coefficients R, S, T_1, T_2 in each trig (39). Of course, application of the double Fourier series in its traditional form leads to the same result, but it is much more cumbersome. The vector function $\mathbf{g}$ is expressed in a similar way

$$\begin{aligned}\mathbf{g}(x,y)=\sum_{s,t=0}^{\infty}\Bigg(&a_{st}^{-}\frac{\partial\mathrm{trig}_{st}(R_{st},S_{st},T_{1st},T_{2st};x,y)}{\partial x},\\ &b_{st}^{-}\frac{\partial\mathrm{trig}_{st}(R_{st},S_{st},T_{1st},T_{2st};x,y)}{\partial y},c_{st}^{-}\mathrm{trig}_{st}(R_{st},S_{st},T_{1st},T_{2st};x,y)\Bigg).\end{aligned} \tag{43}$$

Let us note that Eqs. (40) and (43) contain the same trigs (with the same parameters R_{st}, S_{st}, T_{1st} and T_{2st}) with different coefficients $a_{st}^{\pm}$, $b_{st}^{\pm}$, $c_{st}^{\pm}$. There is no contradiction in the representations (40) and (43), because one can gather all trigs from $\mathbf{f}$ and $\mathbf{g}$, and generate the series for $\mathbf{f}$ and $\mathbf{g}$ with zeros at the appropriate locations.

After these preliminaries, we can construct a solution of the Stokes equation with the boundary conditions corresponding to each trigonometrical term of Eqs. (40) and (43). Let us fix a term

$$\mathrm{trig}_{st}\equiv\mathrm{trig}_{st}(R_{st},S_{st},T_{1st},T_{2st};x,y).$$

We consider the Stokes equations

$$\begin{aligned}&\nabla^2\mathbf{U}_{st}=\nabla Q_{st},\\ &\nabla\cdot\mathbf{U}_{st}=\mathbf{0}\end{aligned} \tag{44}$$

with the boundary conditions at $z=\pm b$

$$\begin{aligned}&\mathbf{U}_{st}(x,y,b)=\left(a_{st}^{+}\frac{\partial\mathrm{trig}_{st}}{\partial x},b_{st}^{+}\frac{\partial\mathrm{trig}_{st}}{\partial y},c_{st}^{+}\mathrm{trig}_{st}\right),\\ &\mathbf{U}_{st}(x,y,-b)=\left(a_{st}^{-}\frac{\partial\mathrm{trig}_{st}}{\partial x},b_{st}^{-}\frac{\partial\mathrm{trig}_{st}}{\partial y},c_{st}^{-}\mathrm{trig}_{st}\right).\end{aligned} \tag{45}$$

For definiteness, we take $s\neq 0$ and $t\neq 0$. We look for $\mathbf{U}_{st}$ and Q_{st} in the form

$$\begin{aligned}&\mathbf{U}_{st}(x,y,z)=\left(\alpha_{st}(z)\frac{\partial\mathrm{trig}_{st}(x,y)}{\partial x},\beta_{st}(z)\frac{\partial\mathrm{trig}_{st}(x,y)}{\partial y},\gamma_{st}(z)\mathrm{trig}_{st}(x,y)\right),\\ &Q_{st}(x,y,z)=\delta_{st}(z)\mathrm{trig}_{st}(x,y),\end{aligned} \tag{46}$$

where $\alpha_{st}(z)$, $\beta_{st}(z)$, $\gamma_{st}(z)$ and $\delta_{st}(z)$ are unknown functions of z. Substituting Eqs. (46) into Eqs. (44), we obtain the system of ordinary differential equations analogous to Eqs. (29)–(31):

$$\begin{aligned}
&\alpha''_{st}(z) - (s^2+t^2)\alpha_{st}(z) - \delta_{st}(z) = 0,\\
&\beta''_{st}(z) - (s^2+t^2)\beta_{st}(z) - \delta_{st}(z) = 0,\\
&\gamma''_{st}(z) - (s^2+t^2)\gamma_{st}(z) - \delta'_{st}(z) = 0,\\
&\gamma'_{st}(z) - s^2\alpha_{st}(z) - t^2\beta_{st}(z).
\end{aligned} \tag{47}$$

Substitution of Eqs. (46) into Eqs. (45) yields the boundary conditions for Eqs. (47):

$$\alpha_{st}(\pm b) = a^{\pm}_{st}, \quad \beta_{st}(\pm b) = b^{\pm}_{st}, \quad \gamma_{st}(\pm b) = c^{\pm}_{st}. \tag{48}$$

The following calculations, which are quite tedious, could be performed in a symbolic way. Mathematica was used systematically, but in a semiautomatic way. We obtain the solution of Eqs. (47)–(48) in closed form (compare with Eq. (38)):

$$\begin{aligned}
\alpha_{st}(z) &= \frac{1}{\varkappa^2_{st}}\left(\gamma'_{st}(z) + t^2 M(z)\right),\\
\beta_{st}(z) &= \frac{1}{\varkappa^2_{st}}\left(\gamma'_{st}(z) - s^2 M(z)\right),\\
\gamma_{st}(z) &= (C_1 z + C_2)\cosh z + (C_3 z + C_4)\sinh z,\\
\delta_{st}(z) &= 2(C_1\cosh z + C_3 \sinh z),
\end{aligned} \tag{49}$$

where

$$\begin{aligned}
C_1 &= \frac{(c^+_{st} - c^-_{st})\cosh b - (d^+_{st} + d^-_{st})\sinh b}{2b - \sinh 2b},\\
C_2 &= \frac{b(c^+_{st} + c^-_{st})\cosh b + \left(c^+_{st} + c^-_{st} - b(d^+_{st} - d^-_{st})\right)\sinh b}{2b + \sinh 2b},\\
C_3 &= \frac{(d^+_{st} - d^-_{st})\cosh b - (c^+_{st} + c^-_{st})\sinh b}{2b + \sinh 2b},\\
C_4 &= \frac{\left(-c^+_{st} + c^-_{st} + b(d^+_{st} + d^-_{st})\right)\cosh b - b(c^+_{st} - c^-_{st})\sinh b}{2b - \sinh 2b},\\
M(z) &= \frac{M^+_{st} + M^-_{st}}{\cosh \varkappa_{st} b}\cosh \varkappa_{st} z - \frac{M^+_{st} - M^-_{st}}{\sinh \varkappa_{st} b}\sinh \varkappa_{st} z,
\end{aligned}$$

and

$$\begin{aligned}
&\varkappa_{st} = \sqrt{s^2 + t^2},\\
&M^+_{st} = a^+_{st} - b^+_{st}, \quad M^-_{st} = a^-_{st} - b^-_{st},\\
&d^+_{st} = s^2 a^+_{st} + t^2 b^+_{st}, \quad d^-_{st} = s^2 a^-_{st} + t^2 b^-_{st}.
\end{aligned}$$

Here, the constants $C_1, \ldots, C_4$ correspond to undetermined constant in the two-dimensional case (see Eq. (38)). The functions $\mathbf{U}_{st}$ have the form (46) and are the solution of the problem (24)–(25)

$$\mathbf{v}(x,y,z) = \sum_{s,t=0}^{\infty} \mathbf{U}_{st}(x,y,z). \tag{50}$$

Finally, we should note that we have constructed $\mathbf{U}_{st}(x,y,z)$ for non-zero s and t. The cases $s=0$ or (and) $t=0$ can be studied by the same method. We do not explicit the derivation and the results here. However, we use these results in the computations below.

The interested reader can look at Appendix A where the ε–expansion of the velocities is shown to converge for $\varepsilon \le \varepsilon_c = (b\varkappa)^{-1}$, where $\varkappa$ is the maximal wave number of $T(x,y)$ and $B(x,y)$.

3.3 Permeability

In Subsect. 3.2, we have proposed an algorithm to construct $\mathbf{v}(x,y,z)$, satisfying Eqs. (24)–(25). Hence, it is possible to calculate $\mathbf{u}_m(x,y,z)$ satisfying Eqs. (22)–(23). In the present subsection, we calculate the permeability K expressed by Eq. (10) by using $\mathbf{u}_m(x,y,z)$. The main goal is to avoid direct calculations of the integrals in Eq. (10).

It follows from Sect. 3.2 that the x-component of $\mathbf{u}_m$ is represented as follows:

$$u_m(x,y,z) = \sum_{s,t=0}^{\infty} a_{m,sk}(z)\mathrm{trig}_{m,st}(x,y), \tag{51}$$

where $\mathrm{trig}_{m,st}(x,y)$ is an abbreviation which stands for

$$\mathrm{trig}_{m,st}(x,y) = \mathrm{trig}_{st}\big(\alpha_{m,st},\beta_{m,st},\gamma_{m,st},\delta_{m,st};x,y\big).$$

Let us substitute Eq. (51) into Eq. (10):

$$K_x = -\frac{\mu}{\overline{\nabla p}\,|\tau|}\sum_{m=0}^{\infty}\varepsilon^m \sum_{s,t=0}^{\infty}\int_{-\pi}^{\pi}\int_{-\pi}^{\pi}\mathrm{trig}_{m,st}(x,y)dxdy \int_{-b(1+\varepsilon B)}^{b(1+\varepsilon T)} a_{m,st}(z)dz. \tag{52}$$

First, we consider the integral

$$J = \int_{-b(1+\varepsilon B)}^{b(1+\varepsilon T)} a(z)dz = A(b+\varepsilon bT) - A(-b-\varepsilon bB), \tag{53}$$

where $A(z)$ is a primitive function of $a(z)$. Let us expand $A(z)$ as a Taylor series

$$A(b+\varepsilon bT) = \sum_{m=0}^{\infty}\frac{A^{(m)}(b)}{m!}(b\varepsilon T)^m = A(b) + \sum_{m=1}^{\infty}\frac{a^{(m-1)}(b)}{m!}b^m T^m \varepsilon^m,$$

$$A(-b-\varepsilon bB) = A(-b) + \sum_{m=1}^{\infty}\frac{a^{(m-1)}(-b)}{m!}(-b)^m B^m \varepsilon^m,$$

where $a^{(m-1)}$ is the derivative of order $(m-1)$ of $a(z)$. Then, Eq. (53) becomes

$$J = \int_{-b}^{b} a(z)dz + \sum_{m=1}^{\infty}\frac{b^m\varepsilon^m}{m!}\Big(T^m(x,y)a^{(m-1)}(b) - (-1)^m B^m(x,y)a^{(m-1)}(-b)\Big). \tag{54}$$

Let us substitute Eq. (54) into Eq. (52):

$$K_x = -\frac{\mu}{\overline{\nabla p}\,|\tau|}\sum_{m=0}^{\infty}\varepsilon^m\sum_{n=0}^{m}\frac{b^n}{n!}J_{m-n,n}, \tag{55}$$

where

$$J_{m,n} := \sum_{s,t=0}^{\infty} \left(\left(a_{m,st}^{(n-1)}(b) J_{m,n,st} - (-1)^n a_{m,st}^{(n-1)}(-b) J_{m,-n,st} \right) \right),$$

$$J_{m,0,00} := \mathrm{trig}_{m,00} \int_{-b}^{b} a_{m,00}(z)dz,$$

$$J_{m,0,st} := 0 \quad \text{for} \quad s^2 + t^2 \neq 0, \tag{56}$$

$$J_{m,n,st} := \int_{-\pi}^{\pi} \int_{-\pi}^{\pi} T^n(x,y)\mathrm{trig}_{m,st}(x,y)dxdy \quad \text{for} \quad n > 0,$$

$$J_{m,-n,st} := \int_{-\pi}^{\pi} \int_{-\pi}^{\pi} B^n(x,y)\mathrm{trig}_{m,st}(x,y)dxdy \quad \text{for} \quad n > 0.$$

Here, $\mathrm{trig}_{m,00}$ is a constant:

$$\begin{aligned} \mathrm{trig}_{m,00} &= \mathrm{trig}_{00}\left(\alpha_{m,00}, \beta_{m,00}, \gamma_{m,00}, \delta_{m,00}; x, y\right) \\ &= \left(\alpha_{m,00}\cos(sx+ty) + \beta_{m,00}\sin(sx+ty)\right. \\ &\quad \left. + \gamma_{m,00}\cos(sx-ty) + \delta_{m,00}\sin(sx-ty)\right)\big|_{s=t=0} = \alpha_{m,00} + \gamma_{m,00}. \end{aligned}$$

The formula (55) will be applied in the following computations. Let us note that we have to calculate only one ordinary integral $J_{m,0,00}$. The integrals $J_{m,n,st}$ are equal to the zeroth coefficients of the Fourier series of integrands, because of the orthogonality of the trigonometric functions involved. A symbolical-numerical algorithm has been constructed to extract the zeroth Fourier terms from $T^n(x,y)\mathrm{trig}_{m,st}(x,y)$.

4 Examples

This section intends to provide various applications of the general technique; it will also illustrate its major advantages.

4.1 Symmetric sinusoidal two-dimensional channel

Let us consider the two-dimensional channel bounded by the surfaces

$$z = b(1 + \varepsilon\cos x), \quad z = -b(1 + \varepsilon\cos x). \tag{57}$$

This example is the most studied in the references cited in Sect. 1. We perform calculations for $b = 0.5$ preserving the parameter ε in symbolic form. The permeability is calculated up to $O(\varepsilon^{32})$:

$$\begin{aligned} K(\varepsilon) = 1 - \sum_{n=1}^{\infty} c_{2n}\varepsilon^{2n} &= K_{30}(\varepsilon) + O(\varepsilon^{32}) = 1 - 3.14963\varepsilon^2 + 4.08109\varepsilon^4 \\ &- 3.48479\varepsilon^6 + 2.93797\varepsilon^8 - 2.56771\varepsilon^{10} + 2.21983\varepsilon^{12} - 1.93018\varepsilon^{14} \\ &+ 1.67294\varepsilon^{16} - 1.45302\varepsilon^{18} + 1.26017\varepsilon^{20} - 1.09411\varepsilon^{22} + 0.949113\varepsilon^{24} \\ &- 0.823912\varepsilon^{26} + 0.714804\varepsilon^{28} - 0.620463\varepsilon^{30} + O(\varepsilon^{32}). \end{aligned} \tag{58}$$

The general advantages of this expansion are clear. First, this analytical expression is valid for a wide range of values of ε; if one wishes to obtain permeability with a precision equal to 10^{-3}, the previous expression is valid up to $\varepsilon = 0.8$. Second, the flow field is itself obtained analytically with the same precision; we shall use this important feature in Sect. 4.4.

Let us briefly compare the present results with what can obtain a finite difference code such as the one described by [1] which can be summarized as follow. In order to cope with the continuity equation, the so-called artificial compressibility method was applied with a staggered maker and cell (MAC) mesh. In essence, the problem is replaced by an unsteady compressible one which is assumed to converge towards the steady incompressible situation of interest. It is obvious that to derive Eq. (58) with the same precision with this code would require a very large computational effort; moreover, for small values of ε, an equivalent precision could not be obtained by a finite difference code.

A specific bonus of having an analytical formula such as Eq. (58) can be discussed. One can note that the coefficients c_{2n} in Eq. (58) for $n \geqslant 4$ satisfy the law

$$c_{2n} = C_0(-q)^{-n} \tag{59}$$

with $C_0 = 5.19679$ and $q = 1.15220$ (see Fig. 3) calculated by the least square method. Using this rule and the condition $K(1) = 0$, we can extend Eq. (58) by adding terms of the form (59). Then, the full expansion for the permeability can be summed and we obtain

$$K(\varepsilon) = K_{30}(\varepsilon) + \frac{\alpha\varepsilon^{32}}{\beta + \varepsilon^2}, \tag{60}$$

where $\alpha = 0.604220$ and $\beta = 1.09880$ are calculated again by the least square method. The functions $K(\varepsilon)$ and $K_{30}(\varepsilon)$ are displayed in Fig. 4 where they are seen to superpose exactly; these results are also in perfect agreement with numerical calculations (cf. [4]).

A lubrication approximation in the case of two cylinders of different radii that are almost in contact with one another along a line was recalled in [1]. For equal radii a, the flow rate q per unit length is proportional to the pressure variation Δp:

$$q = -\frac{K_l}{\mu}\Delta p, \tag{61}$$

where K_l is given by

$$K_l = \frac{2}{9\pi}\sqrt{\frac{\delta^5}{a}} \tag{62}$$

and δ is the gap between the cylinders.

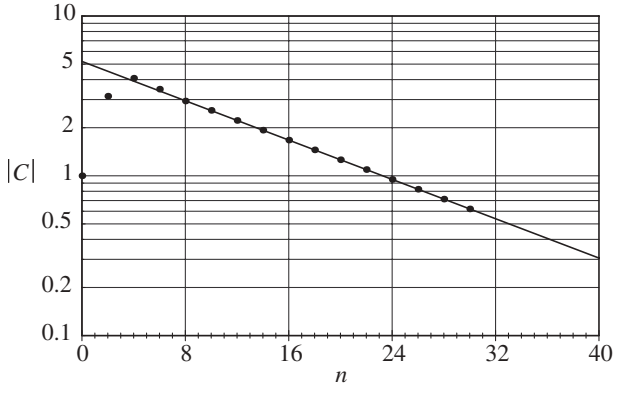

Fig. 3. The coefficients $|c_{2n}|$ (cf. Eq. (58)) as functions of n. The solid line is the expression (59)

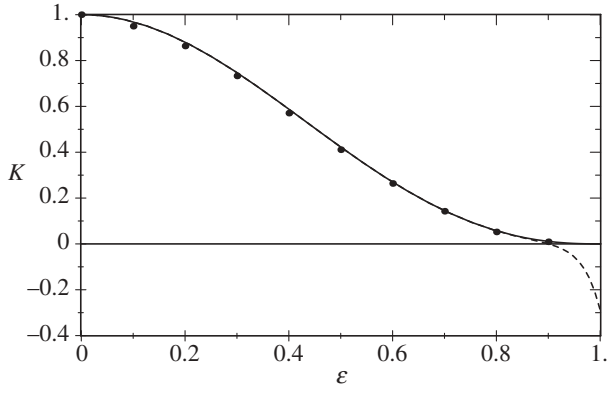

Fig. 4. The normalized permeability K as a function of ε for the channel defined by Eq. (57) with $b = 0.5$. Data are for: solid line: Eq. (60); broken line: Eq. (58); dots: numerical solution.

For the channel (57), if ε is close to unity, the aperture at $x = -\pi$ is close to zero. Hence, one can apply Eq. (62) to this local channel with $\delta = 2b(1-\varepsilon)$ and $a = b\varepsilon$. The functions $K_l(\varepsilon)$ and $K(\varepsilon)$ are compared in Fig. 5 near $\varepsilon = 1$; the lubrication approximation (62) is seen to be good for ε close to 0.99, while for smaller ε it is too large.

Let us consider now the channel bounded by the surfaces (57) with $b = 0.25$. $K(\varepsilon)$ is readily obtained as

$$\begin{aligned} K(\varepsilon) = 1 &- 3.03748\varepsilon^2 + 3.54570\varepsilon^4 - 2.33505\varepsilon^6 + 1.35447\varepsilon^8 \\ &- 0.83303\varepsilon^{10} + 0.49762\varepsilon^{12} - 0.30350\varepsilon^{14} + 0.18185\varepsilon^{16} \\ &- 0.11083\varepsilon^{18} + 0.06636\varepsilon^{20} - 0.04051\varepsilon^{22} + 0.02419\varepsilon^{24} \\ &- 0.01483\varepsilon^{26} + 0.00880\varepsilon^{28} - 0.00544\varepsilon^{30} + O(\varepsilon^{32}). \end{aligned} \tag{63}$$

Burns and Parkes [6] have derived the same values for the coefficients of $K(\varepsilon)$ up to $O(\varepsilon^6)$. A comparison of Eq. (63) with the results of [6] is presented in Fig. 6.

4.2 Parallel sinusoidal two-dimensional channel

The present channel is bounded by the surfaces

$$z = b(1 + \varepsilon\cos x), \quad z = -b(1 - \varepsilon\cos x) \tag{64}$$

with $b = 0.5$. The permeability is calculated up to $O(\varepsilon^{32})$:

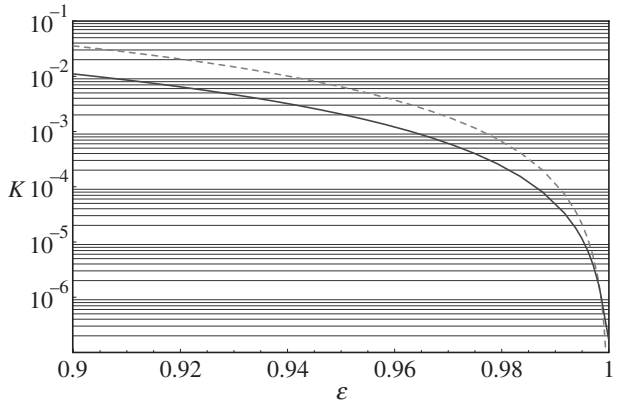

Fig. 5. The permeability K as a function of ε near $\varepsilon = 1$ in logarithmic scale for the channel defined by Eq. (57) with $b = 0.5$. Data are for: solid line: Eq. (60); broken line lubrication solution, Eq. (62).

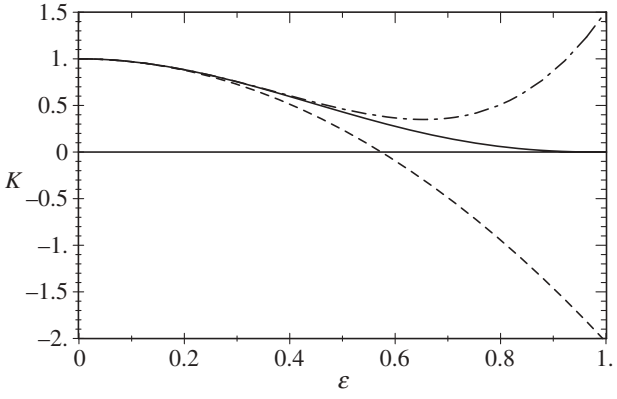

Fig. 6. The permeability K as a function of ε for the channel defined by Eq. (57) with $b = 0.25$. Data are for: solid line: Eq. (63); broken line: the second-order approximation $K_2(\varepsilon)$ of [6]; dotted-broken line: the fourth-order approximation $K_4(\varepsilon)$ of [6].

$$\begin{aligned} K_{30}(\varepsilon) = 1 &- 2.53686 \times 10^{-1}\varepsilon^2 + 4.28907 \times 10^{-2}\varepsilon^4 - 5.46188 \times 10^{-3}\varepsilon^6 \\ &+ 4.54695 \times 10^{-4}\varepsilon^8 + 9.0656 \times 10^{-6}\varepsilon^{10} - 1.41572 \times 10^{-5}\varepsilon^{12} \\ &+ 3.76584 \times 10^{-6}\varepsilon^{14} - 6.72021 \times 10^{-7}\varepsilon^{16} + 7.58331 \times 10^{-8}\varepsilon^{18} \\ &+ 2.34495 \times 10^{-9}\varepsilon^{20} - 4.59993 \times 10^{-9}\varepsilon^{22} + 1.88446 \times 10^{-9}\varepsilon^{24} \\ &- 8.6005 \times 10^{-11}\varepsilon^{26} + 3.34156 \times 10^{-9}\varepsilon^{28} + 1.63748 \times 10^{-9}\varepsilon^{30}. \end{aligned} \tag{65}$$

The velocity is analytic in ε in the disk $|\varepsilon| < \varepsilon_c$. Therefore, Eq. (65) is valid for $\varepsilon < \varepsilon_c$. In order to calculate $K(\varepsilon)$ for $\varepsilon \geqslant \varepsilon_c$, one can apply a Padé approximation [24] to the polynomial (65) which agrees up to $O(\varepsilon^{32})$. We take the Padé approximation of the order $(10, 20)$

$$K(\varepsilon) = \frac{P_{10}(\varepsilon)}{Q_{20}(\varepsilon)}, \tag{66}$$

where

$$\begin{aligned} P_{10}(\varepsilon) &= 1 - 3.14215\varepsilon^2 + 6.59346\varepsilon^4 + 34.7591\varepsilon^6 + 13.3065\varepsilon^8 + 1.53446\varepsilon^{10}, \\ Q_{20}(\varepsilon) &= 1 - 2.88846\varepsilon^2 + 5.81781\varepsilon^4 + 36.3643\varepsilon^6 + 22.2659\varepsilon^8 + 5.65641\varepsilon^{10} \\ &\quad + 0.675967\varepsilon^{12} + 0.033858\varepsilon^{14} + 0.000131\varepsilon^{16} - 0.000010\varepsilon^{18} + 0.000001\varepsilon^{20}. \end{aligned} \tag{67}$$

$K(\varepsilon)$ is displayed in Fig. 7.

We have also performed pure numerical computations of the permeability for the same channel. It turned out that to obtain a precise result a fine discretization mesh is neccessary; N_C denotes the number of mesh points along the z-axis; Fig. 7 shows that the discrepancy between the numerical and analytical results decreases with N_C and that the agreement becomes acceptable for $N_C \geqslant 230$.

It is possible to check that Eq. (66) and Padé approximations of other orders provide similar results for $\varepsilon \leqslant 8$. Let us note that in this case the amplitude of the oscillatory part of the channel exceeds its width by a factor 8, i.e., ε is certainly not a small parameter anymore.

These last two remarks further illustrate the advantages of the present technique as they were discussed in Sect. 4.1.

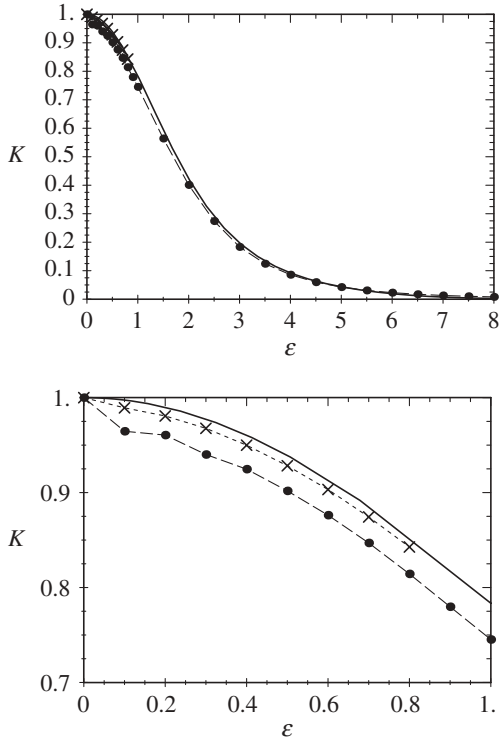

Fig. 7. The permeability $K(\varepsilon)$ for the channel defined by Eq. (64) with $b = 0.5$. Data are for: solid line: Eq. (66); dots: numerical solution with $N_C = 50$; crosses: numerical solution with $N_C = 230$. The second graph presents an enlarged view close to $\varepsilon = 0$.

4.3 Symmetric sinusoidal three-dimensional channel

Let us consider the channel restricted by the surfaces

$$z = \pm b\left(1 + \frac{1}{2}\varepsilon(\cos(x+y) + \cos(x-y))\right) \tag{68}$$

with $b = 0.3$. The permeability is calculated up to $O(\varepsilon^{14})$ as

$$\begin{aligned} K_{14}(\varepsilon) = 1 &- 0.465674\varepsilon^2 + 0.329218\varepsilon^4 - 0.261666\varepsilon^6 \\ &- 0.004467\varepsilon^8 - 0.0386987\varepsilon^{10} - 0.0177808\varepsilon^{12} - 0.0239319\varepsilon^{14}. \end{aligned} \tag{69}$$

For $\varepsilon = 1$, the surfaces (68) start touching though the permeability is not yet zero (see Fig. 8). In this case, the order $O(\varepsilon^{16})$ provides a sufficient precision since the lower-order formulas give close results.

Therefore, permeability is obtained with a precision of 10^{-3} for values of ε up to 0.61. Again, for low values of ε, the corresponding precision can be hardly obtained with a standard numerical code since the velocity field is three-dimensional.

4.4 Eddies in a channel

This section illustrates the obvious fact that the velocity field is derived with the same precision as the permeability. Again this field is given by an expression valid up to large values of ε as we repeatedly

stressed. This is a very interesting feature since these fields can be used to study a long list of phenomena such as the onset of eddies, a topic which is closely related to the generation of turbulence.

The present section is devoted to this phenomenon in the two-dimensional channel bounded by the surfaces

$$z = b, \quad z = -b(1 + \varepsilon \cos x). \tag{70}$$

with $b = \frac{\pi}{2}$. According to (A.7), the critical value ε_c for this channel is equal to $\frac{2}{\pi}$. Using the algorithm presented in Subsect. 3.1 and 3.2, the x–component of the velocity is given by

$$u(x,z) = \sum_{m=0}^{26} u_m(x,z)\varepsilon^m + O(\varepsilon^{27}), \tag{71}$$

where the successive $u_m(x,z)$ can be detailed as

$$\begin{aligned}
u_0(x,z) &= 2.46740 - z^2, \\
u_1(x,z) &= -(0.962707\cosh z + 0.842888 z\cosh z \\
&\quad - 0.37143\sinh z - 1.35081 z\sinh z)\cos x, \\
u_2(x,z) &= -3.48573 + 2.21909 z + (0.12526\cosh 2z + 0.263130 z\cosh 2z \\
&\quad - 0.11304\sinh 2z - 0.27219 z\sinh 2z)\cos 2x, \\
u_3(x,z) &= (2.37210\cosh z + 0.37807 z\cosh z - 1.70666\sinh z \\
&\quad - 0.97226 z\sinh z)\cos x + (-0.04006\cosh 3z - 0.08828 z\cosh 3z \\
&\quad + 0.03980\sinh 3z + 0.08847 z\sinh 3z)\cos 3x, \\
&\ldots
\end{aligned} \tag{72}$$

We write here only three terms, but all the 26 terms are used to calculate the Padé approximations applied to Eq. (71) on ε. The results are presented in Fig. 9. In order to investigate $u(x,z)$ near the bottom wall, we consider the point $P\{x = 0, z = -b(1+\varepsilon) + \frac{b}{10}\}$ for which Eq. (71) is reduced to

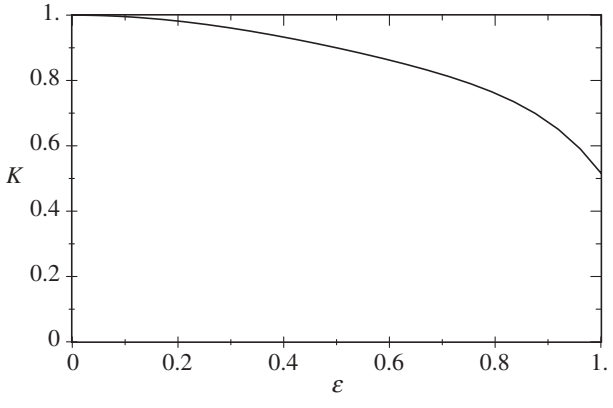

Fig. 8. The approximation $K_{14}(\varepsilon)$ calculated with Eq. (69) for the permeability of the channel defined by Eq. (68)

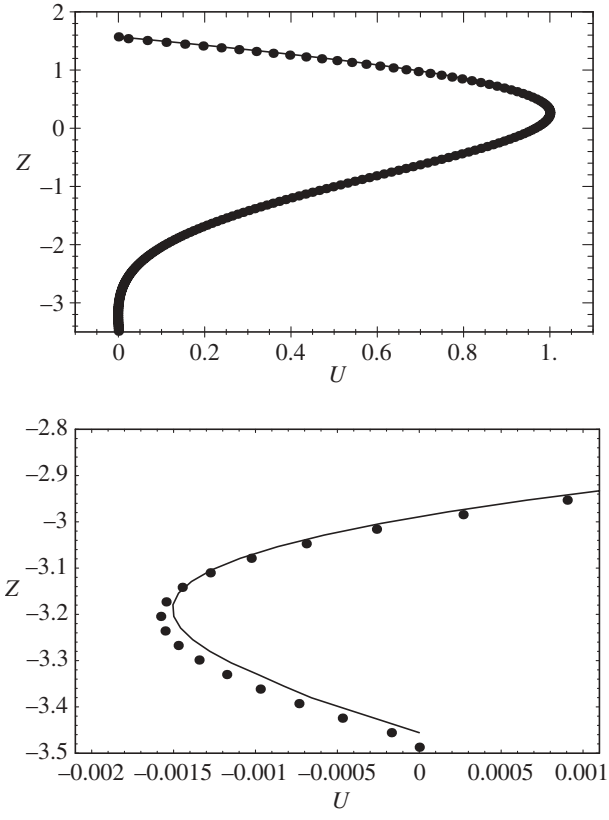

Fig. 9. The x-component of velocity on the profile $x = 0$, $-3.4558 \leqslant z \leqslant 1.5708$ for the channel defined by Eq. (70) with $b = \pi/2$. Data are for: solid line: the Padé approximation of order $(13, 13)$ applied to Eq. (71); dots: numerical solution. A fragment of the profile near $z = -3$ is presented in the second picture.

$$
\begin{aligned}
u_P(\varepsilon) = u[0, -b(1+\varepsilon) + \frac{b}{10}, \varepsilon] &= 0.46881 - 0.96803\varepsilon - 0.52896\varepsilon^2 + 1.75422\varepsilon^3 \\
&+ 1.73336\varepsilon^4 - 3.17184\varepsilon^5 - 4.75907\varepsilon^6 + 5.86634\varepsilon^7 + 11.30828\varepsilon^8 \\
&- 11.30390\varepsilon^9 - 25.34523\varepsilon^{10} + 22.85543\varepsilon^{11} + 55.78013\varepsilon^{12} - 47.95656\varepsilon^{13} \\
&- 122.65423\varepsilon^{14} + 103.07507\varepsilon^{15} + 271.14318\varepsilon^{16} - 224.97244\varepsilon^{17} \\
&- 603.49792\varepsilon^{18} + 496.32144\varepsilon^{19} + 1352.20577\varepsilon^{20} - 1104.20681\varepsilon^{21} \\
&- 3048.22737\varepsilon^{22} + 2474.27540\varepsilon^{23} + 6909.26971\varepsilon^{24} \\
&- 5579.58252\varepsilon^{25} - 15738.87145\varepsilon^{26}.
\end{aligned} \tag{73}
$$

Further, we apply the Padé approximations of the orders $(k, 26-k)$ $(k = 8, 9, 10, 11, 12)$ in ε to Eq. (73). For instance, the Padé approximation $(10, 16)$ has the form $P_{10}(\varepsilon)/Q_{16}(\varepsilon)$, where

$$
\begin{aligned}
P_{10}(\varepsilon) &= 0.4688 - 0.6732\varepsilon + 2.4885\varepsilon^2 - 3.7506\varepsilon^3 + 5.1133\varepsilon^4 - 6.8634\varepsilon^5 + 5.4600\varepsilon^6 \\
&- 4.3419\varepsilon^7 + 2.6469\varepsilon^8 - 0.4522\varepsilon^9 - 0.0996\varepsilon^{10}, \\
Q_{16}(\varepsilon) &= 1 + 0.6289\varepsilon + 7.7352\varepsilon^2 + 4.9397\varepsilon^3 + 23.784\varepsilon^4 + 15.5412\varepsilon^5 + 37.8959\varepsilon^6 \\
&+ 25.4686\varepsilon^7 + 34.8549\varepsilon^8 + 23.6913\varepsilon^9 + 20.0401\varepsilon^{10} + 12.6700\varepsilon^{11} \\
&+ 7.7389\varepsilon^{12} + 3.8726\varepsilon^{13} + 1.899\varepsilon^{14} + 0.7117\varepsilon^{15} + 0.1887\varepsilon^{16}.
\end{aligned} \tag{74}
$$

The Padé approximations are presented in Fig. 10. One can see that various Padé approximations of Eq. (73) give the same result near $\varepsilon = 1$. In particular, one can see that $u_P(\varepsilon) > 0$ for $\varepsilon < 1$ and that $u_P(\varepsilon)$ is negative from $\varepsilon = 1$ to a point $\varepsilon \sim 1.5$. These negative values of $u_P(\varepsilon)$ imply that eddies will be generated for ε greater than 1. Therefore, for this channel, we have $\varepsilon_e = 1$ while the critical value of convergence ε_c is equal to $\frac{2}{\pi}$ as an application of Eq. (A.7). The streamlines of the velocity field for $\varepsilon = 1.2$ are displayed in Fig. 11. Numerical calculations of velocity performed for the same channel gave very close results (see Fig. 9).

We have performed the same analysis for the channel defined by Eq. (70) with $b = 1$. In this case, we have $\varepsilon_c = 1$ and $\varepsilon_e = \frac{\pi}{2}$. Hence, we can conjecture that for this type of channel $\varepsilon_e = \frac{\pi}{2}\varepsilon_c = \frac{\pi}{2b}$. This implies that the onset of eddies depends only on the shape of the bottom wall and does not depend on the width of the channel. The critical bottom surface is determined by the relation $z = -b(1 + \varepsilon_e \cos x) = -b - \frac{\pi}{2}\cos x$.

One can go a little further in these qualitative observations. It seems that for the Poiseuille flow, ε_e is always larger than ε_c. However, the opposite seems to be true for the disturbed Couette flow (see [25] and [15]).

4.5 Eddies in a parallel sinusoidal channel with large amplitudes

Let us apply the previous analysis to the two-dimensional channel bounded by the surfaces (64), but now with $b = 2$. It follows from Eq. (A.7) that the critical value ε_c for this channel is equal to 0.5.

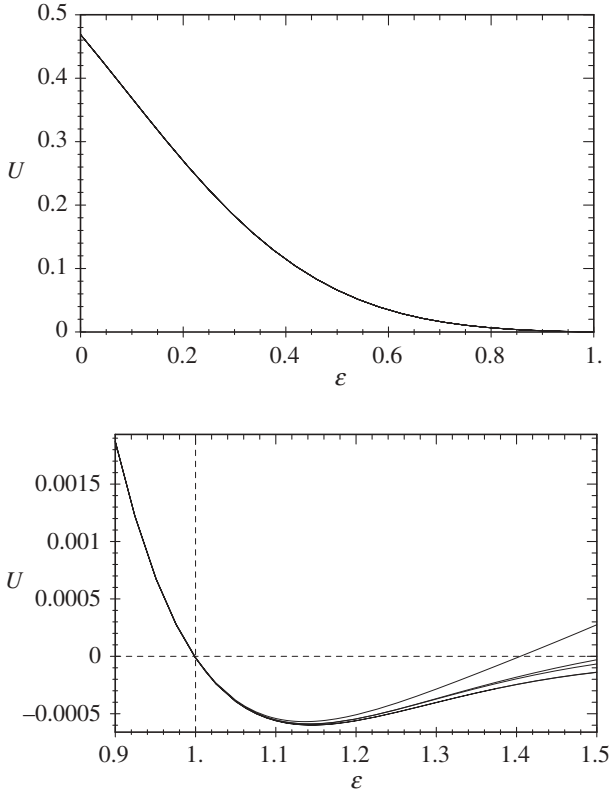

Fig. 10. Various Padé approximations applied to the x-component of the velocity (73) at the point $P\{x = 0, z = -b(1 + \varepsilon) + \frac{b}{10}\}$ for the channel defined by Eq. (70) with $b = \pi/2$

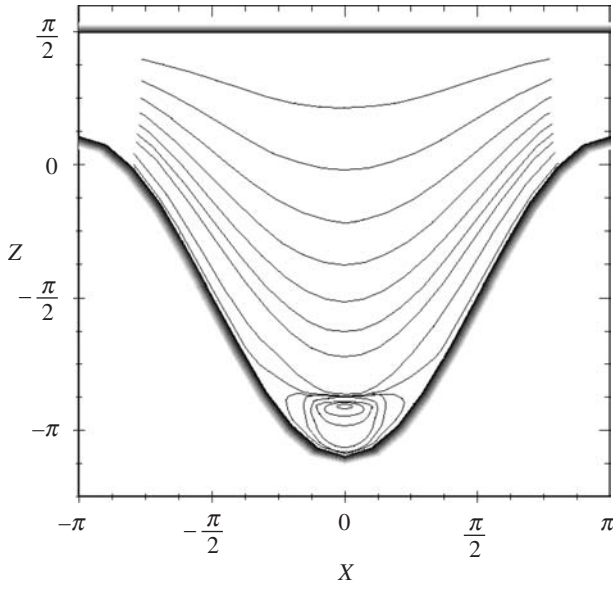

Fig. 11. The streamlines in the channel defined by Eq. (70) with $b = \pi/2$ and $\varepsilon = 1.2$ constructed by the Padé approximations of the velocity field (71)–(72)

Using the algorithm presented in Sects 3.1 and 3.2, we calculate the x-component of the velocity,

$$u(x,z) = \sum_{m=0}^{30} u_m(x,z)\varepsilon^m + O(\varepsilon^{31}), \tag{75}$$

where $u_m(x,z)$ can be written in explicit form. As in Subsect. 4.4, we apply Padé approximations to Eq. (75). Velocity profiles $u(0,z)$ for $-b(1+\varepsilon) \leqslant z \leqslant b(1+\varepsilon)$ are presented in Fig. 12 for various ε. One can see that in the channel defined by (64) there is no eddy. Actually, the calculations were performed up to $\varepsilon = 1000$ with an unknown precision; even in such an extreme case, no eddy could be obtained.

The physical meaning of these results is quite clear. For sufficiently small values of b, the velocity profile becomes progressively parabolic for large values of ε as it is seen in Fig. 12.

However, one may expect eddies when b is large; this possibility was not further explored in this paper.

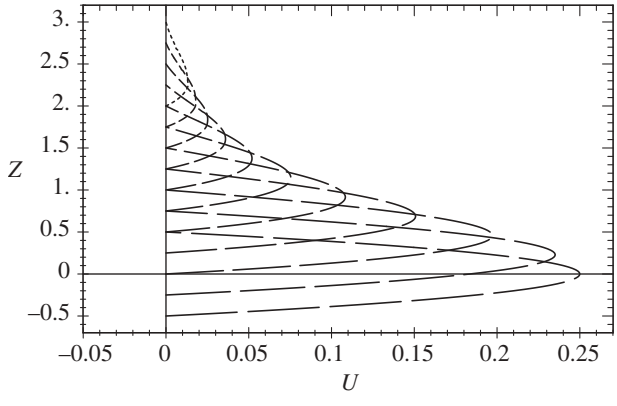

Fig. 12. The x-component of velocities in the points $x = 0$, $-b(1+\varepsilon) \leqslant z \leqslant b(1+\varepsilon)$ for $\varepsilon = 0, 0.5, \ldots, 5$ for the channel defined by Eq. (64) with $b = 0.5$. The greater lengths of the segments in lines correspond to the smaller values of ε.

5 Analytical formulas up to $O(\varepsilon^4)$

In Subsect. 3.1–3.3, we have constructed a general algorithm to calculate the permeability K up to a given accuracy $O(\varepsilon^{m+1})$. When Eq. (A.1) is fulfilled, Eq. (23) implies that the application of the algorithm up to $O(\varepsilon^{m+1})$ is possible if the functions $\mathbf{u}_n(x,y,z)$ are differentiable $(m-n)$ times in z $(n=1,2,\ldots,m-1)$, i.e., $\mathbf{u}_n \in C^{m-n}$ $(n=1,2,\ldots,m-1)$. Let us note that the zeroth approximation $\mathbf{u}_0$ (16) is infinitely differentiable in z. However, the smoothness of the next approximations depends on the smoothness of $T(x,y)$ and $B(x,y)$. Let us demonstrate this property for the two-dimensional channel defined by Eqs. (3) and (4) in the form of pointwise convergent Fourier series

$$T(x) = \sum_{m=1}^{\infty} \alpha_m \cos mx + \beta_m \sin mx,$$

$$B(x) = \sum_{m=1}^{\infty} \gamma_m \cos mx + \delta_m \sin mx. \tag{76}$$

Let us apply the general formula (55) to calculate K up to $O(\varepsilon^4)$. We have

$$K \approx 1 - \frac{3\varepsilon^2}{2b^2}\left(I_{2,0} + bI_{1,1} + \frac{1}{2}b^2 I_{0,2}\right), \tag{77}$$

where after some symbolic computations we obtain

$$I_{0,2} = S, \quad I_{1,1} = -bS, \quad I_{2,0} = \frac{1}{2b}\int_{-b}^{b} a_{20}(z)dz,$$

$$S := \frac{1}{2}\sum_{m=1}^{\infty}\left(\alpha_m^2 + \beta_m^2 + \gamma_m^2 + \delta_m^2\right). \tag{78}$$

Calculation of a_{20} in accordance with the algorithm and substitution of Eqs. (78) into Eq. (77) yield the following analytical formula valid up to $O(\varepsilon^4)$:

$$K \approx 1 - \frac{3}{4}\varepsilon^2 \sum_{m=1}^{\infty}\left(F_1(mb)\left(\alpha_m^2 + \beta_m^2 + \gamma_m^2 + \delta_m^2\right) + F_2(mb)(\alpha_m\gamma_m + \beta_m\delta_m)\right), \tag{79}$$

where

$$F_1(z) := \frac{-1 + \cosh 4z - 2z\sinh 4z}{1 + 8z^2 - \cosh 4z},$$

$$F_2(z) := \frac{8z(2z\cosh 2z - \sinh 2z)}{1 + 8z^2 - \cosh 4z}.$$

In order to investigate the convergence of Eq. (79), let us note that $F_1(z) \sim 2z$ and that $F_2(z)$ tends to zero as $z \to \infty$. Hence, the series (79) converges iff the following series converges:

$$\sum_{m=1}^{\infty} m\left(\alpha_m^2 + \beta_m^2 + \gamma_m^2 + \delta_m^2\right). \tag{80}$$

The formula (79) is written for the length of the channel $L = \pi$. By a scale change, it is easy to rewrite Eq. (79) for arbitrary L:

$$K = 1 - \frac{3}{4}\varepsilon^2 \sum_{m=1}^{\infty}\left(F_1\left(\frac{mb\pi}{2L}\right)\left(\alpha_m^2 + \beta_m^2 + \gamma_m^2 + \delta_m^2\right) + F_2\left(\frac{mb\pi}{2L}\right)(\alpha_m\gamma_m + \beta_m\delta_m)\right) + O(\varepsilon^4). \tag{81}$$

Note that for a symmetric channel, i.e., $B(x) = T(x)$, Eq. (79) becomes

$$K \approx 1 + \frac{3}{2}\varepsilon^2 \sum_{m=1}^{\infty} \frac{2mb\cosh 2mb - \sinh 2mb}{2mb - \sinh 2mb} \left(\alpha_m^2 + \beta_m^2\right). \tag{82}$$

It is important to note that in principle higher orders of ε can be obtained. However, the resulting formulae with all parameters in symbolic form are extremely long and the present limitations of the computers and of the software are almost reached.

5.1 Comparison with previous works

Let us first compare special cases of Eq. (81) with previous works obtained by others. At the end of Sect. 4.1, we have already compared our results with [6] for the symmetric sinusoidal channel.

Hasegawa and Izuchi [9] obtained a formula for the sinusoidal-flat channel

$$S^+ = \frac{1}{2} - \varepsilon\cos x, \quad S^- = -\frac{1}{2}, \tag{83}$$

which in our designations reads as

$$K = 1 - \left(33 + \frac{13}{2695}\mathscr{R}e^2\right)\frac{\varepsilon^2}{40} + O(\varepsilon^4), \tag{84}$$

where $\mathscr{R}e$ is the Reynolds number. Equation (84) with $\mathscr{R}e = 0$ becomes

$$K = 1 - 0.825\varepsilon^2 + O(\varepsilon^4), \tag{85}$$

which corresponds to Eq. (81) with $b = 0.5$, $L = 0.5$ and $\alpha_1 = -2$ (all other coefficients $\alpha_m, \beta_m, \gamma_m, \delta_m$ in Eq. (81) are zero):

$$K = 1 - 3\varepsilon^2 F_1(0.5) \approx 1 - 0.851\varepsilon^2 + O(\varepsilon^4). \tag{86}$$

The difference between Eqs. (85) and (86) is explained by the assumption in [9] that $\varepsilon \ll L$. In the limit $L \to \infty$, we derive from [9] and Eq. (81) the same result $K = 1 - 3\varepsilon^2 + O(\varepsilon^4)$.

5.2 The Weierstrass function

This function is defined as [26]

$$W_H(x) := \sum_{n=1}^{\infty} A^{-nH}\cos A^n x, \tag{87}$$

where $A > 1$. We assume that $\frac{1}{2} < H < 1$. The function $W_H(x)$ has the following properties:

(i) the series (87) converges absolutely and uniformly to $W_H(x)$ on $\mathbb{R}$,
(ii) $W_H(x)$ is continuous, but nowhere differentiable.

Let us discuss some aspects of Eq. (82). We take a symmetric channel to simplify calculations. The property ii) implies that the channel bounded by the walls (87) has an irregular geometry which implies complex flows near the walls. Let us check the condition (A.1). For this two–dimensional channel, we have $\Lambda_n = A^{-nH}$ and $\varkappa_n = A^n$, hence

$$\sup_n |\Lambda_n|\varkappa_n = \sup_n A^{n(1-H)} = +\infty, \tag{88}$$

since $A > 1$ and $H < 1$. This implies that the series (18) are divergent for any $\varepsilon > 0$.

However, it is proved in Appendix B that the approximations up to $O(\varepsilon^2)$ of the velocity are correctly defined even for this complicated fractal channel and therefore the permeability can be calculated by the general formula (82) which for the walls $T(x,y) = B(x,y) = W_H(x)$ reads as follows:

$$K \approx 1 + \frac{3}{2}\varepsilon^2 \sum_{n=1}^{\infty} \frac{2bA^n \cosh 2bA^n - \sinh 2bA^n}{2bA^n - \sinh 2bA^n} A^{-2nH}. \tag{89}$$

6 Lubrication approximation

Many estimates of channel permeability based on the assumption that the lubrication approximation is valid locally, have been proposed. One can find an extensive review in [2]. This approximation is characterized by the fact that the amplitude of the wall oscillations is smaller than the channel width. It turns out that the channel width is small when compared to a characteristic length of the channel, i.e., $\varepsilon \ll b \ll 2\pi$ in our notations. The main assumption is that the velocity has a parabolic profile.

The lubrication approximation of the flow between two cylindrical surfaces that are almost in contact, has been discussed in Sect. 4.1. The present section is devoted to a comparison between the parabolic profiles of the velocity and the permeability obtained in the framework of the lubrication approximation for plane channels and the rigorous method based on the Stokes equation presented in Sects. 3.1–3.3. Following [2], let us recall the main formulas for the lubrication approximation; the pressure $p = p(x,y)$ satisfies the Reynolds equation

$$\nabla \cdot \left(h^3 \nabla p\right) = 0, \tag{90}$$

where the aperture of the channel $h(x,y) := S^+(x,y) - S^-(x,y)$ is calculated as

$$h(x,y) = 2b(1 + \varepsilon S(x,y)), \quad S(x,y) = \frac{1}{2}(T(x,y) + B(x,y)). \tag{91}$$

Equation (90) is considered for a class of functions periodic in x and y with periods 2π. The velocity has a parabolic profile in z:

$$\mathbf{u} \approx \frac{1}{2}(z - S^+(x,y))(z - S^-(x,y))\overline{\nabla p}, \tag{92}$$

where $\overline{\nabla p}$ is the applied pressure gradient.

The real velocity profiles $\mathbf{u}$ obtained by the rigorous method presented in Subsects. 3.1–3.3 for the channel bounded by Eq. (57) are presented in Fig. 13. Disturbances are observed when ε increases. For $\varepsilon \sim 0.8$, regions where convergence is not reached appear. The Padé approximation is not applied in order to improve the validity of the results in this example. Let us find the best parabolas approximating $\mathbf{u}$; for each fixed x (y is absent since a two-dimensional channel is considered), it is chosen as the parabola which minimizes the relative error

$$\sigma = \left(\sum_{i=1}^{N} \left(\frac{u_i - v_i}{u_{\max}} \right)^2 \right)^{1/2}, \tag{93}$$

where u_i are the values of the x-component of $\mathbf{u}$ at the points along the vertical section of the channel; v_i are the values of the best parabola. The error (93) as a function of ε is presented in Fig. 14 for the channel defined by Eq. (57).

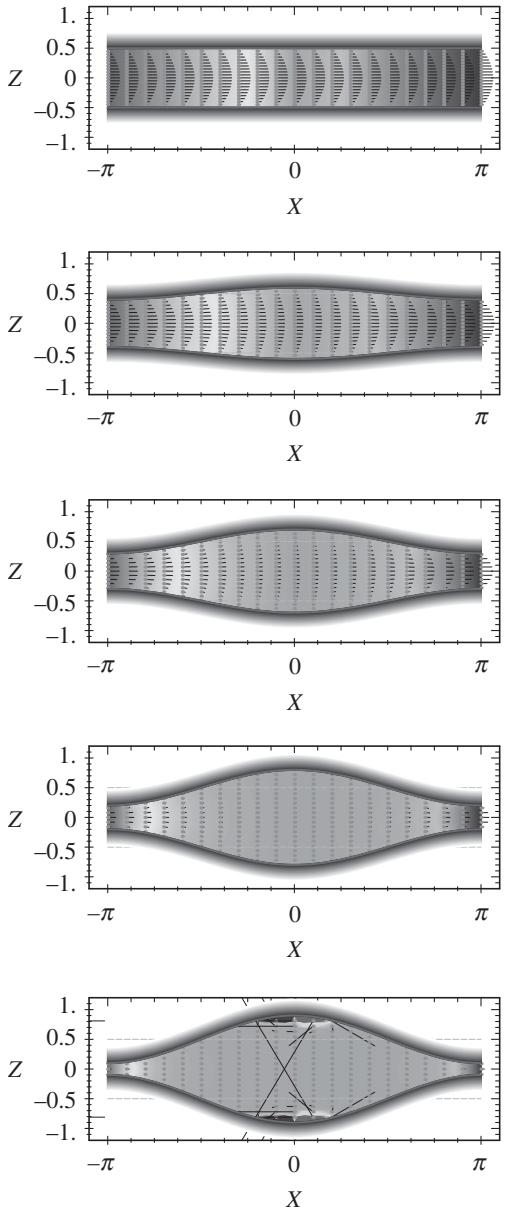

Fig. 13. Velocity profiles for the channel defined by Eq. (57) for $\varepsilon = 0, 0.2, 0.4, 0.6, 0.8$. $\varepsilon = 0$ corresponds to the straight channel with parabolic profiles.

Using the approximation (92), we obtain the Reynolds permeability in the x-direction

$$K_R = -\frac{1}{12 \cdot 8\pi^2 b} \int_{-\pi}^{\pi} \int_{-\pi}^{\pi} h^3(x,y) \frac{\partial p}{\partial x} dx dy. \tag{94}$$

Here, we use Eq. (10) and Eq. (3.120) from [2]. In order to determine K_R, we have to find p from the Reynolds equation (90). It is possible to solve Eq. (90) by a method presented in [27]. For simplicity, we now consider the one-dimensional Reynolds equation

$$\frac{d}{dx}\left(h^3(x)\frac{dp}{dx}\right) = 0. \tag{95}$$

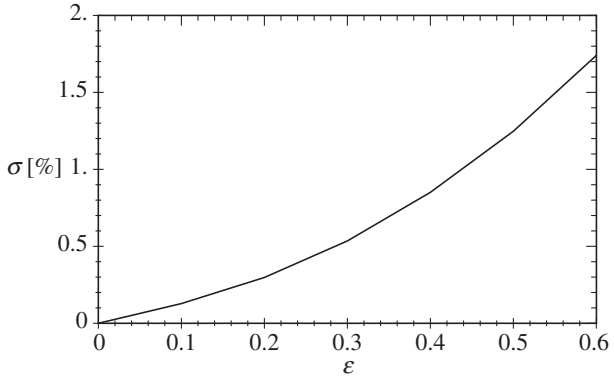

Fig. 14. The error $\sigma = \sigma(\varepsilon)$ calculated with Eq. (93) for the channel defined by Eq. (57)

This ordinary differential equation (95) is solved with the boundary condition

$$\overline{\nabla p} = \int_{-\pi}^{\pi} \frac{dp}{dx} dx. \tag{96}$$

To calculate K_R, we need only $h^3(x)\frac{dp}{dx}$. Standard manipulations yield

$$h^3(x)\frac{dp}{dx} = 8b^3\overline{\nabla p}\left(\int_{-\pi}^{\pi} \frac{dx}{\big(1+\varepsilon S(x)\big)^3}\right)^{-1}. \tag{97}$$

Then, Eq. (94) becomes

$$K_R(\varepsilon) = -\frac{b^2\overline{\nabla p}}{3}\left(\int_{-\pi}^{\pi} \frac{dx}{\big(1+\varepsilon S(x)\big)^3}\right)^{-1}. \tag{98}$$

In order to be consistent with the normalized permeability (17), we calculate $K_R(\varepsilon)/K_R(0)$.

One can see in Fig. 15 that Eq. (98) is in agreement with Eq. (63) for the symmetric sinusoidal channel (57). For parallel channels, we have $S(x,y) = 0$; hence, Eq. (98) does not depend on ε and it is not in agreement with formula (65) for the channel (63) (see Fig. 16).

Therefore, the lubrication approximation (98) gives correct results only for channels in which the mean surface $S(x,y) = b + \frac{\varepsilon}{2}(T(x,y) - B(x,y))$ is sufficiently close to a plane and for small value of ε. This conclusion is in agreement with [17] and [19].

7 Conclusion

The main result of this paper is to provide analytical expressions for the velocities **u** and the permeability K of curvilinear channels. We use a method based on the ε–expansions of **u** and K which was applied up to $O(\varepsilon^N)$ for small N in previous papers for particular two-dimensional channels. Symbolic computations enable us to construct an analytical-numerical algorithm for solving boundary value problems for the straight channel. This algorithm can be applied to an arbitrary three-dimensional channel with practically arbitrary precision. In some examples, calculations were performed up to $O(\varepsilon^{32})$.

As results, one obtains analytical expressions for the velocity and the pressure fields, as well as for integral quantities such as permeabilities. These expressions possess several advantages

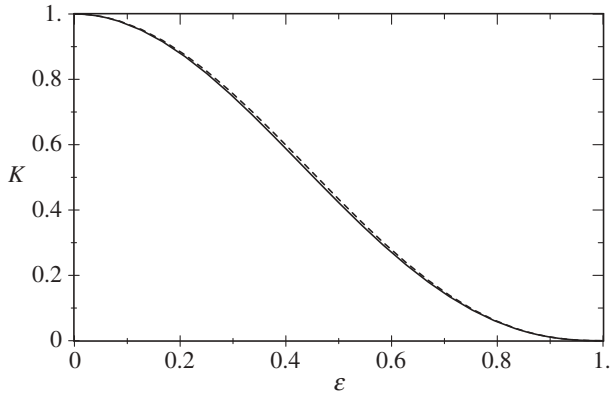

Fig. 15. The permeability as a function of ε for the channel defined by Eq. (57). Data are for: solid line: Eq. (60); broken line: Eq. (98).

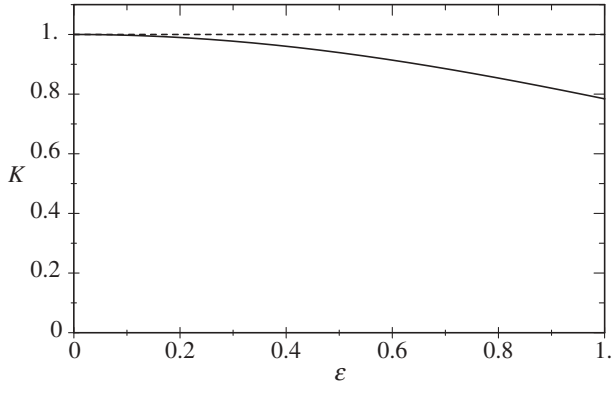

Fig. 16. The permeability as a function of ε for the channel defined by Eq. (64). Data are for: solid line: Eq. (65); broken line: Eq. (98).

over numerical calculations performed by standard techniques which are discussed in the text. Often a similar precision cannot be obtained by these codes.

These fields can then be used in further studies. The stability of these analytical velocity fields in wavy channels and their dependence on the Reynolds number can be studied in a straightforward way using similar expansions on ε.

Other important phenomena require the knowledge of the velocity field such as dispersion and electro-osmosis. We are presently extending our work in all these directions.

Appendix A: Convergence of the algorithm

In the present appendix, we investigate the convergence of the algorithm described in Sect. 3.1. We now wish to know up to which ε we may use the expansion (18).

First, we note that the solution of the problem (24)–(25) is infinitely differentiable for the infinitely differentiable functions $T(x,y)$ and $B(x,y)$. In particular, the derivatives in z are correctly defined in Eqs. (20)–(21) and consequently in Eq. (23). Existence and uniqueness of $\mathbf{u}_m$ and p_m follow from the cascade (22)–(23). However, this does not address the convergence of Eq. (18) in ε. Therefore, we have to study the right-hand side of Eq. (23) in order to estimate $\mathbf{u}_m$ and then the convergence of Eq. (18). At the beginning we consider the case where $T(x,y)$ and $B(x,y)$ are trigonometric polynomials. We shall prove in Subsect. A.1 that ε must be less than a value of order $(b\varkappa)^{-1}$ where $\varkappa$ is the maximal wave number of $T(x,y)$ and $B(x,y)$. The

estimation of the domain of convergence in the general case is given in Subsect. A.2. We shall establish that the algorithm converges if

$$\varepsilon < \varepsilon_c = \left[b \sup_{st} \Lambda_{st} \sqrt{s^2 + t^2} \right]^{-1}, \tag{A.1}$$

where Λ_{st} is the maximal number of modulus of eight coefficients of $T(x,y)$ and $B(x,y)$ in expansion in the double Fourier series on four basic functions $\cos(sx+ty), \ldots, \sin(sx-ty)$.

A.1 Convergence of the algorithm for polynomials

Let us establish the following auxiliary result concerning the solution $\mathbf{v}$ of the problem (24)–(25): *Let $\varkappa_{\max}$ be the maximal wave number of $\mathbf{f}$ and $\mathbf{g}$ with the corresponding amplitude A. Then, $\partial^p \mathbf{v}/\partial z^p$ is of order $A\varkappa^p$*:

$$\frac{\partial^p \mathbf{v}}{\partial z^p} \sim A\varkappa^p. \tag{A.2}$$

To prove this property, we use the series (40) and (43), as well as the explicit forms (46) and (49) of the solver. Let us fix a triplet from Eqs. (40) and (43)

$$\left(a_{st}^{\pm} \frac{\partial \mathrm{trig}_{st}(R_{st}, S_{st}, T_{1st}, T_{2st}; x, y)}{\partial x}, b_{st}^{\pm} \frac{\partial \mathrm{trig}_{st}(R_{st}, S_{st}, T_{1st}, T_{2st}; x, y)}{\partial y}, \right.$$
$$\left. c_{st}^{\pm} \mathrm{trig}_{st}(R_{st}, S_{st}, T_{1st}, T_{2st}; x, y) \right) \tag{A.3}$$

with the amplitudes

$$\left(a_{st}^{\pm}, b_{st}^{\pm}, c_{st}^{\pm}\right). \tag{A.4}$$

The triplet (A.3) yields the solution $\mathbf{U}_{st}$ of Eq. (45) with the amplitudes

$$(\alpha_{st}(z), \beta_{st}(z), \gamma_{st}(z)) \tag{A.5}$$

written in the form (49). One can see from Eq. (49) that all the amplitudes $\alpha_{st}(z)$, $\beta_{st}(z)$, $\gamma_{st}(z)$ depend linearly on the constants $C_1, \ldots, C_4$ which are also linearly dependent on $a_{st}^{\pm}$, $b_{st}^{\pm}$, $c_{st}^{\pm}$. Hence, $\alpha_{st}(z)$, $\beta_{st}(z)$, $\gamma_{st}(z)$ are linearly dependent on $a_{st}^{\pm}$, $b_{st}^{\pm}$, $c_{st}^{\pm}$. Therefore, the amplitudes (A.5) are of the same order as the amplitudes (A.4). The amplitudes of the derivatives

$$\left(\alpha_{st}^{(p)}(z), \beta_{st}^{(p)}(z), \gamma_{st}^{(p)}(z)\right), \quad p = 1, 2, \ldots \tag{A.6}$$

are of order $\varkappa_{st}^p$ where $\varkappa_{st} = \sqrt{s^2 + t^2}$. This follows from the calculation of the derivatives of the amplitudes (A.5) via $M(z)$ (see Eq. (49)), since the terms $\cosh \varkappa_{st} z$ and $\sinh \varkappa_{st} z$ in $M(z)$ yield the multiplier $\varkappa_{st}$ after each differentiation. The determination of the maximum on s and t yields the desired asymptotic equation (A.2).

An important consequence of Eq. (A.2) can be stated as follows: *If ε verifies*

$$\varepsilon < \varepsilon_c = (b\varkappa)^{-1}, \tag{A.7}$$

where $\varkappa := \max_{s,t} \varkappa_{st}$ is the maximal wave number of $T(x,y)$ and $B(x,y)$, the ε-expansion (18) converges absolutely and uniformly in $S^+(x,y) \leqslant z \leqslant S^-(x,y)$.

This can be proved by the application of Eq. (A.2) to each step of the cascade (22)–(23). Let us consider Eq. (23) with $m = 1$:

$$\mathbf{u}_1(x, y, b) = 2b^2 T(x, y), \quad \mathbf{u}_1(x, y, -b) = -2b^2 B(x, y). \tag{A.8}$$

Then, $\partial^p \mathbf{u}_1/\partial z^p$ is of order $b^2\varkappa^p$. The next $\mathbf{u}_m$ are investigated by induction on m separately by the variables z (by the parameter $\varkappa$) and (x,y) (by the parameter b).

First, we fix b. Let $\partial^p \mathbf{u}_n/\partial z^p$ be of order $\varkappa^{n+p-1}$ $(n=1,2,\ldots,m-1)$. Then, Eq. (5) and the boundary condition (23) imply that

$$|\mathbf{u}_m(x,y,\pm b)| \leqslant \sum_{n=1}^{m-1} \frac{b^n}{n!} \left| \frac{\partial^n \mathbf{u}_{m-n}}{\partial z^n} \right|_{z=\pm b} \sim e^b \varkappa^{m-1}.$$

It follows from Eq. (A.2) for $p=0$ that the velocity $\mathbf{u}_m(x,y,z)$ in the channel has the same order as on the boundary $\mathbf{u}_m(x,y,\pm b)$. Therefore,

$$\mathbf{u}_m \sim \varkappa^m. \tag{A.9}$$

Let us now fix $\varkappa$ and estimate the order of $\mathbf{u}_m$ on b. As it follows from Eqs. (44) and (45), $\mathbf{U}_{st}(x,y,z)$ is linearly dependent on the boundary amplitudes $a_{st}^{\pm}$, $b_{st}^{\pm}$, $c_{st}^{\pm}$. Moreover, Eqs. (46) and (49) imply that $\frac{\partial^p \mathbf{U}_{st}}{\partial z^p}(x,y,z)$ preserves the order on b. Hence, all the functions $\frac{\partial^p \mathbf{u}_m}{\partial z^p}(x,y,z)$ $(p=0,1,\ldots)$ have the same order. Equation (A.8) implies that $\mathbf{u}_1 \sim b^2$. Let us assume that $\mathbf{u}_n \sim b^{n+1}$ for $n=1,2,\ldots,m-1$. Then, Eq. (23) yields

$$\mathbf{u}_m \sim \sum_{n=1}^{m-1} \frac{b^n}{n!} b^{m-n+1} \leqslant b^{m+1} e.$$

This relation together with Eq. (A.9) implies that $\mathbf{u}_m$ is of order $(b\varkappa)^m$. Then, the rate of convergence of Eq. (18) is bounded by $\varepsilon b\varkappa$ and Eq. (18) converges for $\varepsilon b\varkappa < 1$. This proves Eq. (A.7).

A.2 Convergence of the general algorithm

We now consider the general case, when $T(x,y)$ and $B(x,y)$ are expanded in double Fourier series. Let $\mathrm{trig}_1(x,y)$, $\mathrm{trig}_2(x,y),\ldots$ be a linearly ordered sequence of the basic functions $\cos(sx+ty),\ldots,\sin(sx-ty)$ (see Eq. (39)). Then $T(x,y)$ and $B(x,y)$ can be represented in the form

$$\begin{aligned} T^*(x,y) &= \varepsilon b T(x,y) = \sum_{s=1}^{\infty} \varepsilon_{2s} \mathrm{trig}_s(x,y), \\ B^*(x,y) &= \varepsilon b B(x,y) = \sum_{s=1}^{\infty} \varepsilon_{2s-1} \mathrm{trig}_s(x,y), \end{aligned} \tag{A.10}$$

where for convenience the Fourier coefficients of the both boundary profiles $T(x,y)$ and $B(x,y)$ are also linearly ordered, ε_1, $\varepsilon_2,\ldots$.

Instead of the expansion (18), we use the series

$$\begin{aligned} p(x,y,z) &= \sum_{N=0}^{\infty} \sum_{m_1,\ldots,m_N} p_{m_1,\ldots,m_N} \varepsilon_1^{m_1} \ldots \varepsilon_N^{m_N}, \\ \mathbf{u}(x,y,z) &= \sum_{N=0}^{\infty} \sum_{m_1,\ldots,m_N} \mathbf{u}_{m_1,\ldots,m_N} \varepsilon_1^{m_1} \ldots \varepsilon_N^{m_N}. \end{aligned} \tag{A.11}$$

This means that instead of the parameter ε in Eq. (18) we consider all the ε_j $(j=1,2,\ldots)$ as perturbation parameters. We use the formula (compare with Eq. (19))

$$g(x,y,b+T^*(x,y)) = \sum_{m=0}^{\infty} \frac{1}{m!} \left(\sum_{s=0}^{\infty} \varepsilon_{2s} \mathrm{trig}_s(x,y) \right)^m \frac{\partial^m g}{\partial z^m}\Big|_{z=b}. \tag{A.12}$$

Application of Eq. (A.12) to (A.11) yields

$$\mathbf{0} = \mathbf{u}(x, y, b + T^*(x, y)) = \sum_{N=0}^{\infty} \sum_{m=0}^{\infty} \sum_{m_1,\ldots,m_N} \frac{1}{m!} \left(\sum_{s=0}^{\infty} \varepsilon_{2s} \mathrm{trig}_s(x, y) \right)^m \frac{\partial^m \mathbf{u}}{\partial z^m} \Big|_{z=b} \varepsilon_1^{m_1} \ldots \varepsilon_N^{m_N}, \tag{A.13}$$

Selecting in Eq. (A.13) the coefficients on the terms $\varepsilon_1^{m_1}\ \varepsilon_2^{m_2} \ldots$, where $m_j = 0, 1, \ldots$, we obtain a boundary condition of the type

$$\mathbf{u}_{m_1,\ldots,m_N}(x, y, b) = \sum_{m, n_1,\ldots,n_N} c_{m,n_1,\ldots,n_N} \frac{\partial^m \mathbf{u}_{n_1,\ldots,n_N}}{\partial z^m} \Big|_{z=b}, \tag{A.14}$$

where $c_{m,n_1,\ldots,n_N}$ are some coefficients. One can obtain a similar boundary condition for $z = -b$. Thus, we obtain a tree–cascade of the boundary value problems for the Stokes equations. To each problem from cascade a sequence $(m_1, m_2, \ldots)$ is assigned. In order to solve a problem corresponding to a fixed sequence $(m_1, m_2, \ldots)$, we have to solve problems $(n_1, n_2, \ldots)$ for $n_1 = 0, 1, \ldots, m_1$; $n_2 = 0, 1, \ldots, m_2$; ….

First, consider a sub-cascade with a nonzero element at place j $(0, \ldots, 0, m, 0, \ldots)$ with $m = 0, 1, 2, \ldots$. In each step of the sub–cascade, we follow the ε-algorithm from Sect. 3 with $\varepsilon = b^{-1}\varepsilon_j$. Subsection A.1 implies that the sub-cascade yields a convergent series if the inequality

$$|\varepsilon_j| \varkappa_j < 1 \tag{A.15}$$

is fulfilled. Here, the number j corresponds to the linearly ordered set of the basic trigonometric functions. Hence, coming back to the double ordering, one can rewrite Eq. (A.15) in the form (A.1).

Let a sub-cascade contain nonzero elements $j_1, j_2, \ldots$. Then, the sub-cascade yields a convergent series if

$$|\varepsilon_{j_1}| \varkappa_{j_1} |\varepsilon_{j_2}| \varkappa_{j_2} \ldots < 1. \tag{A.16}$$

The latter condition is valid if Eq. (A.15) holds for each j. Therefore, we have proved that the ε-algorithm from Sect. 3 converges if Eq. (A.1) is fulfilled.

The algorithm proposed in this subsection formally generalizes the ε-algorithm from Sect. 3. Actually, the algorithms give the same result. We have presented the general algorithm here only to obtain the estimation (A.1). The ε-algorithm is always applied in computations.

Appendix B: Irregular walls

In the present appendix, we justify the formula (89) in Sect. 5.2.

We are looking for the velocity $\mathbf{u}(x, z)$ in the form

$$\mathbf{u} = \mathbf{u}_0 + \varepsilon \mathbf{u}_1 + \varepsilon^2 \mathbf{u}_2 + O(\varepsilon^4), \tag{B.1}$$

since we need only the terms up to $O(\varepsilon^4)$. According to the general algorithm, $\mathbf{u}_1$ is solution of the equations

$$\nabla^2 \mathbf{u}_1 = \nabla p_1, \quad \nabla \cdot \mathbf{u}_1 = \mathbf{0} \tag{B.2}$$

with the boundary conditions

$$\mathbf{u}_1(x, b) = -bT(x) \frac{\partial \mathbf{u}_0}{\partial z} \Big|_{z=b}, \quad \mathbf{u}_1(x, -b) = bT(x) \frac{\partial \mathbf{u}_0}{\partial z} \Big|_{z=-b}. \tag{B.3}$$

Derive $\partial \mathbf{u}_0/\partial z$ from Eq. (16) and substitute it into Eq. (B.3):

$$\mathbf{u}_1(x, \pm b) = \big(2b^2 T(x), 0\big). \tag{B.4}$$

Following the algorithm, tedious calculations provide the solution of the problem (B.2)–(B.3); for instance, the x-component is written as

$$u_1(x,z) = 2b^2 \sum_{m=1}^{\infty} P_m(z)(\alpha_m \cos mx + \beta_m \sin mx), \tag{B.5}$$

where

$$P_m(z) = 2\frac{(bm\cosh(bm) - \sinh(bm))\cosh(mz) - mz\sinh(bm)\sinh(mz)}{2bm - \sinh(2bm)}.$$

Let us formally calculate the derivative

$$\frac{\partial u_1(x,z)}{\partial z} = 2b^2 \sum_{m=1}^{\infty} P'_m(z)(\alpha_m \cos mx + \beta_m \sin mx). \tag{B.6}$$

Substitute $z = \pm b$ into Eq. (B.6). After simplification, we obtain

$$\begin{aligned} &\frac{\partial u_1}{\partial z}\Big|_{z=b} = 8b^2 \sum_{m=1}^{\infty} \frac{m\sinh^2 mb}{2mb - \sinh 2mb}(\alpha_m \cos mx + \beta_m \sin mx), \\ &\frac{\partial u_1}{\partial z}\Big|_{z=-b} = -\frac{\partial u_1}{\partial z}\Big|_{z=b}. \end{aligned} \tag{B.7}$$

One can see that $P'_m(b)$ for fixed b and large m has the following limit

$$P'_m(b) = \frac{m\sinh^2 mb}{2mb - \sinh 2mb} \sim \frac{m}{2}.$$

Hence, the series (B.7) converges iff the following series converges:

$$\sum_{m=1}^{\infty} m(\alpha_m \cos mx + \beta_m \sin mx). \tag{B.8}$$

Here, we mean the absolute and uniform convergence. The convergence of Eq. (B.8) is stronger than the convergence of Eq. (80). However, we can avoid this additional condition by considering $\partial u_1/\partial z\big|_{z=b}$ as a generalized function. The same convergence problem can be addressed for the velocity inside the channel; the same arguments are valid for $\frac{\partial u_1(x,z)}{\partial z}$.

According to the general algorithm, the next approximation $\mathbf{u}_2$ satisfies the equations

$$\nabla^2 \mathbf{u}_2 = \nabla p_2, \quad \nabla \cdot \mathbf{u}_2 = \mathbf{0} \tag{B.9}$$

with the boundary conditions

$$\mathbf{u}_2\big|_{z=\pm b} = \mp bT \frac{\partial \mathbf{u}_1}{\partial z}\Big|_{z=\pm b} - \frac{b^2}{2} T^2 \frac{\partial^2 \mathbf{u}_0}{\partial z^2}\Big|_{z=\pm b}. \tag{B.10}$$

Calculation of the right-hand part of Eq. (B.10) yields for the x-component

$$u_2(x, \pm b) = b^2T^2 - 8b^2T \sum_{m=1}^{\infty} \frac{mb\sinh^2 mb}{2mb - \sinh 2mb}(\alpha_m \cos mx + \beta_m \sin mx). \tag{B.11}$$

The calculation of K requires only the zeroth term in the Fourier series of $u_2(x, \pm b)$. Therefore, instead of Eq. (B.11), we can consider the conditions

$$u_2^*(x, \pm b) = a,$$

where a is the zeroth term of Eq. (B.11). This constant a yields the coefficient of ε^2 in Eq. (82). The constant a can be considered as a functional which is correctly defined by the assumption that Eq. (80) converges.

In the general case of irregular walls, we have to assume that the functions $T(x)$ and $B(x)$ belong to the Sobolev space $W_2^{\frac{1}{2}}$ (cf. [28]). For instance, all Hölder-continuous functions belong to $W_2^{\frac{1}{2}}$ [29] and the condition of the convergence of the series (80) ($T, B \in W_2^{\frac{1}{2}}$) is sufficient to justify the formula (79). Therefore, we have checked that Eq. (79) can be applied to channels with irregular boundaries.

Acknowledgements

We thank the referee for bringing to our knowledge some important contributions and for his valuable comments. One of us, V. Mityushev, was partially supported by a position of Professeur Invité of IPGP which he acknowledges gratefully.

References

[1] Adler, P. M.: Porous media. Geometry and transport. Oxford: Butterworth-Heinemann 1992.
[2] Adler, P. M., Thovert, J.-F.: Fractures and fracture networks. Oxford: Butterworth-Heinemann 1999.
[3] Mourzenko, V. V., Thovert, J. F., Adler, P. M.: Percolation and conductivity of self-affine fractures. Phys. Rev. E **59**, 4265–4284 (1999).
[4] Mourzenko, V. V., Thovert, J. F., Adler, P. M.: Permeability of self-affine fractures. Transport in Porous Media **45**, 89–103 (2001).
[5] Neira, M. A., Payatakes, A. C.: Collocation solution of creeping Newtonian flow through sinusoidal tubes. AIChE **25**, 725–730 (1979).
[6] Burns, J. C., Parkes, T.: Peristaltic motion. J. Fluid Mech. **29**, 731–743 (1967).
[7] Wang, C. Y.: Stokes flow through a channel with three-dimensional bumpy walls. Phys. Fluids **16**, 2136–2139 (2004).
[8] Deiber, J. A., Schowalter, W. R.: Flow through tubes with sinusoidal axial variations in diameter. AIChE **25**, 638–644 (1979).
[9] Hasegawa, E., Izuchi, H.: On steady flow through a channel consisting of an uneven wall and plane wall. Part 1: Case of no relative motion in two walls. Bull. JSME **26**, 514–520 (1983).
[10] Hasegawa, E., Izuchi, H.: On steady flow through a channel consisting of an uneven wall and plane wall. Part 2: Case of wall with relative velocity. Bull. JSME **27**, 1631–1636 (1984).
[11] Floryan, J. M.: Vortex instability in a diverging-converging channel. J. Fluid Mech. **482**, 17–50 (2003).
[12] Moffatt, H. K.: Viscous and resistive eddies near a sharp corner. J. Fluid Mech **18**, 1–18 (1964).
[13] Moffatt, H. K.: G. K. Batchelor and the homogenization of turbulence. Ann. Rev. Fluid Mech. **34**, 19–35 (2002).
[14] Perspectives in fluid dynamics. In: A collective introduction to current research (Batchelor, G. K., Moffatt, H. K., Worster, M. G., eds.). Cambridge: Cambridge University Press 2000.
[15] Pozrikidis, C.: Creeping flow in two-dimensional channel. J. Fluid Mech. **180**, 495–514 (1987).
[16] Scholle, M., Wierschem, A., Aksel, N.: Creeping films with vortices over strongly undulated channel. Acta Mech. **168**, 167–193 (2004).
[17] Scholle, M.: Creeping Couette flow over an undulated plate. Arch. Appl. Mech. **73**, 823–840 (2004).
[18] Wierschem, A., Scholle, M., Aksel, N.: Vortices in film flow over strongly undulated bottom profiles at low Reynolds numbers. Phys. Fluids **15**, 426–435 (2003).
[19] Gaskell, P. H., Jimack, P. K., Sellier, M., Thompson, H. M., Wilson, M. C. T.: Gravity–driven flow of continuous thin liquid films on non–porous substrates with topography. J. Fluid Mech. **509**, 253–280 (2004).

[20] Zhou, H., Martinuzzi, J. C. , Khayat, R. E. , Straatman, A. G. , Abu-Ramadan, E.: Influence of wall shape on vortex formation in modulated channel flow. Phys Fluids **15**, 3114–3133 (2003).
[21] Bontozoglou, V.: Laminar film flow along a periodic wall. Comp. Model. Eng. Sci. **1**, 133–142 (2000).
[22] Happel, J., Brenner, H.: Low Reynolds number hydrodynamics. New York: Prentice-Hall 1965.
[23] Hinch, E. J.: Perturbation methods. Cambridge: Cambridge University Press 1991.
[24] Baker, G. A.: Padé approximants. Cambridge: Cambridge University Press 1996.
[25] Munson, B. R., Rangwalla, A. A., Mann III, J. A.: Low Reynolds number circular Couette flow past a wavy wall. Phys. Fluids **28**, 2679–2686 (1985).
[26] Gelbaum, B. R., Olmsted, J. M. H.: Theorems and counterexamples in mathematics. New York: Springer 1990.
[27] Adler, P. M., Malevich, A. E., Mityushev, V. V.: Macroscopic diffusion on rough surfaces. Phys. Rev. E. **69**, 011607 (2004).
[28] Zygmund, A. G.: Trigonometric series, vols. I and II combined, 2nd ed. Cambridge: Cambridge University Press 1988.
[29] Kufner, A., Kadles, J.: Fourier series. Prague: Academia 1971.

Authors' addresses: A. E. Malevich, Dept. Mech.-Math., Belarusian State University, pr.F.Skoriny 4, 220050 Minsk, Belarus; V. V. Mityushev, Dept. Math., Pedagogical University, ul. Podchorazych 2, 30-084, Krakow, Poland; P. M. Adler, IPGP, tour 24, 4, place Jussieu, 75252 - Paris Cedex 05, France (E-mail: adler@ipgp.jussieu.fr)